

Populating secluded dark sector with ultra-relativistic bubbles

Aleksandr Azatov^{a,1}, Xander Nagels^{b,2}, Miguel Vanvlasselaer^{c,3}, Wen Yin^{d,4,5}

¹ *SISSA International School for Advanced Studies, Via Bonomea 265, 34136, Trieste, Italy*

² *INFN - Sezione di Trieste, Via Bonomea 265, 34136, Trieste, Italy*

³ *Theoretische Natuurkunde and IIHE/ELEM, Vrije Universiteit Brussel, & The International Solvay Institutes, Pleinlaan 2, B-1050 Brussels, Belgium*

⁴ *Department of Physics, & Tokyo Metropolitan University, Tokyo 192-0397, Japan*

⁵ *Department of Physics, & Tohoku University, Sendai Miyagi 980-8578, Japan*

Abstract

We study Dark Matter production during first order phase transitions from bubble-plasma collisions. We focus on scenarios where the Dark Matter sector is secluded and its interaction with the visible sector (including the Standard Model) originates from dimension-five and dimension-six operators. We find that such DM is generally heavy and has a large initial velocity, leading to the possibility of DM being warm today. We differentiate between the cases of weakly and strongly coupled dark sectors, where, in the latter case, we focus on glueball DM, which turns out to have very distinct phenomenological properties. We also systematically compute the Freeze-In production of the dark sector and compare it with the bubble-plasma DM abundances.

arXiv:2406.12554v1 [hep-ph] 18 Jun 2024

1 Introduction

Phase transitions (PTs) taking place in the early universe, often referred to as *cosmological* phase transitions, received a continuous and growing attention. From a theoretical perspective, since the zero temperature potential is expected to be a complicated manifold with several minima, PTs are considered to be common phenomena within quantum field theory. From a phenomenological perspective, PTs might exhibit intriguing implications for the thermal history of the early universe. In particular, a first order PT (FOPT), where a transition occurs from a metastable to a more stable vacuum state, i.e. to a deeper minimum of the potential, might lead to many phenomenological consequences such as baryogenesis [1–14], the production of heavy dark matter [15–26], primordial black holes [27–31] and possibly observable gravitational waves (GWs) [32–37]. In a related way, FOPTs occur naturally in a large variety of motivated BSM models like composite Higgs [38–42], extended Higgs sectors [43–51], axion models [52, 53], dark Yang-Mills sectors [54, 55] and $B - L$ breaking sectors [56, 57].

The interactions between the bubble wall and the plasma have recently attracted much attention. In the regime of relativistic bubble expansion (BE), when the boost factor $\gamma_w \equiv 1/\sqrt{1 - v_w^2} \gg 1$ (v_w is the velocity of the wall), it was first shown in [58] that the ultra-fast bubble wall could allow exotic $1 \rightarrow 2$ interactions, otherwise forbidden in a Lorentz-invariant background. Subsequently, [59] argued that particles much heavier than the scale of the transition could be produced in $1 \rightarrow 1$ and $1 \rightarrow 2$ processes due to the Lorentz violating bubble wall background and will propagate in shells around the bubble wall. A broad review of the different particle production mechanisms and their corresponding interactions with the bubble wall is given in [60].

It was later suggested [18] that the special class of $1 \rightarrow 2$ processes could lead to the production of heavy scalar Dark Matter (DM) via the operator $\lambda\phi^2 h^2$, where h is the field undergoing the phase transition, potentially playing the role of the Higgs or another scalar field, and ϕ is the heavy DM particle. Due to the large boost factor, reached by ultra-relativistic or runaway bubble walls, DM produced in $h \rightarrow \phi\phi$ transitions will be strongly boosted with an average energy in the plasma frame given by $\bar{E}_{\phi, \text{plasma}} \sim M_\phi^2/T_{\text{nuc}}$, where T_{nuc} is the nucleation temperature and M_ϕ the mass of the scalar ϕ . Based on this realisation, authors of [22] proposed that the bubble wall production mechanism could induce *heavy and warm* Dark Matter (WDM), using again an interaction of the form $\lambda\phi^2 h^2$.

Nevertheless, the DM sector is not necessarily scalar by nature or required to share a renormalizable interaction with the phase transition sector, containing the h field (which in principle could be related to the SM Higgs or not). If the DM sector does not share renormalisable interactions with the SM, it is said to be *secluded*. Such secluded sectors typically interact with the thermal bath via non-renormalisable operators with a characteristic scale Λ , of the type

$$\frac{h^2 \mathcal{O}_{\text{DS}}}{\Lambda^{d-2}}, \quad (1)$$

with \mathcal{O}_{DS} being a function of fields with dimension d , containing the DM candidate. In this paper, we study the production of heavy and potentially warm DM, generated by a phase transition via such non-renormalisable operators in Eq.(1). We assume that the produced particles constitute the entire DM abundance. Consequently, we will see that the phase transition scalar field h *cannot* be the physical SM-like Higgs if the production mechanism is required to produce the observed abundance of DM, but has to be another scalar field, which may be a $B - L$ Higgs boson for the neutrino mass [61–65], a Peccei Quinn Higgs boson [66–69], or some Higgs associated with the flat direction for thermal inflation/supercooling [70, 71]. These Higgs do not have Standard Model gauge charge and it is easy to have an ultra-relativistic bubble wall expansion during the first order phase transition because the friction can be small. Our discussion applies generically, and we denote them as *BSM Higgs*. In what follows, we will denote the SM Higgs with a capital letter H and the BSM Higgs with a lowercase h .

In this paper, we will consider different natures for the DM particle: DM can be a fermion ψ , a dark vector γ or a dark glueball G and we will scrutinize each of these cases in detail. Furthermore, we compute the spectrum of the DM right after bubble production, and track its evolution, taking into account scatterings with the bath. We present schematically our mechanism in Fig. 1, where the

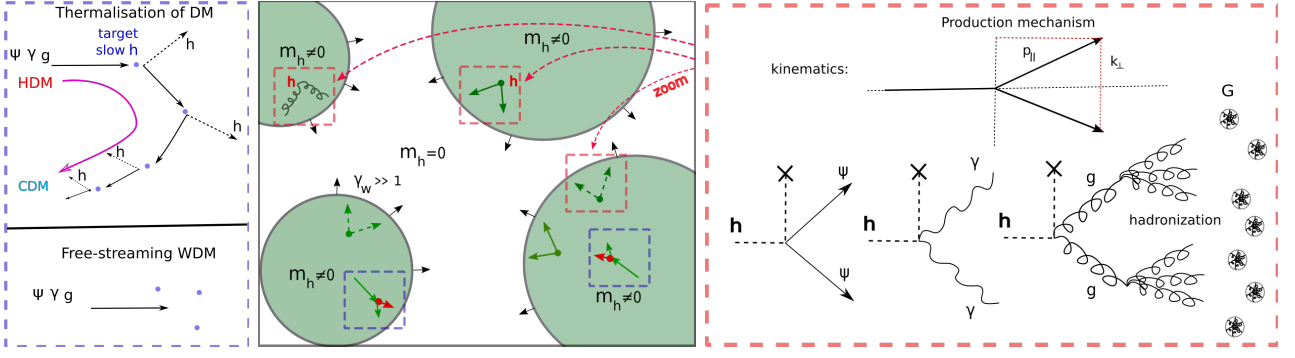


Figure 1: Schematic of the production of Dark Matter from bubbles with $k_{\perp}^2 \sim \gamma_w v T_{\text{nuc}}$, $p_{\parallel} \sim \gamma_w T_{\text{nuc}}$. In the middle panel, we show how the expansion of bubble walls can produce very boosted fermions ψ , vectors γ or gluons g (which become glueballs G) depending on the model under consideration. In the right panel, the red rectangle, we present more in details the bubble-plasma production channels. The cross represents the interaction with the bubble wall which allows the DM production. Subsequently, as shown on the left panel, in the blue rectangle, we show the interactions of the boosted produced particles with the thermalised plasma, the blue h particles on the sketch. The fast ψ, γ, g can interact with the slow targets h via $h(\psi, \gamma, g) \rightarrow h(\psi, \gamma, g)$ and cool down to usual CDM or free-stream and remain warm dark matter. In the main text, we consider either ψ, γ or g to be produced.

production is sketched inside the red rectangle and the rescattering after production inside the blue one.

Here is the summary of the new results presented in this paper:

- We study the production and the abundance of particles originating from a higher-dimensional operator of dimension five and six. We find the following scalings for the corresponding number densities for the production of the particles in the weakly coupled cases: $n_{\text{dim } 5} \propto T_{\text{nuc}}^3 v^2 / \Lambda^2$, $n_{\text{dim } 6} \propto \gamma_w T_{\text{nuc}}^4 v^3 / \Lambda^4$. For the strongly interacting case (glueball DM production), it is more sensible to describe the process in terms of the total energy transferred to the dark sector and we find that the glueball energy density scales as $\rho_G \propto \gamma_w^2 T_{\text{nuc}}^4 v^4 / \Lambda^4$. The scaling of the energy density of the gluons, with the large boost factor, comes from the fact that both the number density of gluons $n_g \propto \gamma_w$ and the energy in the plasma frame of the emitted gluon, $\bar{E}_g \propto \gamma_w$ scale like γ_w .
- For weakly interacting boosted particles, we compute the average velocity at matter-radiation equality and the spectrum of the DM after production, as well as its evolution until matter-radiation equality. Bubble wall production appears to be an efficient mechanism to produce heavy warm DM in both the fermion and the vector production.
- We compute the pressure due to this particle production, which is not only inevitable in our mechanism, but might also be a rather generic effect for FOPTs with fast bubble walls. We find the following relations: $\mathcal{P}_5 \propto \gamma_w v^3 T_{\text{nuc}}^3 / \Lambda^2$ and $\mathcal{P}_6 \propto \gamma_w^2 v^4 T_{\text{nuc}}^4 / \Lambda^4$. We however observe that this pressure is parametrically smaller than the leading order $v^2 T^2$ pressure over the whole range where our computation holds.
- We compute the Freeze-In (FI) abundance produced via the three operators mentioned above and compare with the bubble production via the same operators.

The remainder of this paper is organised as follows: in section 2, we remind the reader of the main results obtained in [18, 22] and highlight the salient characteristics of the scalar emission. In section 3, we present the study of the production of a weakly coupled secluded sector via dimension five and six operators. In section 4, we study the production of high-energy gluons and their confinement leading to glueballs.

2 Reminder of the production via the renormalisable operator

To make our story complete, we first review the computation of the production via the *renormalisable* interaction $\lambda\phi^2 h^2$, as it was initially proposed in [18] and then further studied in [22]. In this section we consider the following Lagrangian

$$\mathcal{L} = \frac{1}{2}(\partial_\mu\phi)^2 - \frac{1}{2}M_\phi^2\phi^2 - \frac{\lambda}{2}h^2\phi^2. \quad (2)$$

During the phase transition, the BSM Higgs field $h \rightarrow h + v$, induces a three-leg vertex in the Lagrangian

$$\mathcal{L} \subset \lambda v h \phi \phi \quad , \quad (3)$$

allowing for splittings $h \rightarrow \phi\phi$. Note that this transition would be forbidden in vacuum and only occurs thanks to the bubble wall presence, which breaks Lorentz invariance, leading to the non-conservation of z -momentum. Using the WKB approximation, the transition from light to heavy states $h \rightarrow \phi\phi$ has a probability of the form [18]¹

$$P_{h \rightarrow \phi^2} \approx \left(\frac{\lambda v}{M_\phi}\right)^2 \frac{1}{48\pi^2} \Theta(1 - \Delta p_z L_w) \simeq \left(\frac{\lambda v}{M_\phi}\right)^2 \frac{1}{48\pi^2} \Theta\left(p_0 - \frac{2M_\phi^2}{v}\right). \quad (4)$$

Where L_w is the width of the wall, which is approximately $L_w \sim 1/v$, with $v \ll M_\phi$, and $\Delta p_z \equiv p_z^h - p_{z,b}^\phi - p_{z,c}^\phi \approx M_\phi^2/(2p_z^h x(1-x)) = 2M_\phi^2/p_z^h$ is the difference of momenta between final- and initial-state particles in the direction orthogonal to the wall, and we took $x = 1/2$ in the last equality. The $\Theta(1 - \Delta p_z L_w)$ -function comes from the requirement that the transition is *non-adiabatic*. Putting a step cut-off is a rough approximation and the exact behaviour is in principle dependent on the wall shape (see Appendix A of [18] and Appendix H of [72] for further discussions). This condition is physically similar to the requirement that the energy in the center-of-mass frame of the collision between a standing particle of the wall and an incoming h , which is $s_{\text{prod}} \sim 2p_0 v$, needs to be larger than $4M_\phi^2$ for on-shell ϕ production.

In the aftermath of the bubble expansion, a non-thermal abundance of ϕ accumulates, which takes the following form

$$\begin{aligned} n_\phi^{\text{BE, PF}} &\approx \frac{2}{\gamma_w v_w} \int \frac{d^3 p}{(2\pi)^3} P_{h \rightarrow \phi^2}(p) \times f_h(p, T_{\text{nuc}}) \\ &\approx \frac{2\lambda^2 v^2}{48\pi^2 M_\phi^2 \gamma_w v_w} \int \frac{d^3 p}{(2\pi)^3} \times f_h(p, T_{\text{nuc}}) \Theta(p_z - 2M_\phi^2/v), \end{aligned} \quad (5)$$

where the subscript PF means evaluated in the plasma frame. $v_w = \sqrt{1 - 1/\gamma_w^2}$ is the velocity of the wall, and $f_h(p)$ is the equilibrium thermal distribution of h outside of the bubble. We assume h to be in thermal equilibrium with the bath at temperature T_{nuc} and is therefore described by a Boltzmann distribution $f_h(p) \approx e^{-\gamma_w(E_h - v_w p_z^h)/T_{\text{nuc}}}$ with $E_h = \sqrt{p_z^2 + \vec{p}_\perp^2}$. We can thus perform the integral in Eq. (5), obtaining

$$n_\phi^{\text{BE}} = \frac{\lambda^2}{96\pi^4 \gamma_w^3 v_w} \times \frac{v^2 T_{\text{nuc}}^2}{M_\phi^2} \left(\frac{M_\phi^2/v}{1 - v_w} + \frac{T_{\text{nuc}}(2 - v_w)}{\gamma_w(v_w - 1)^2} \right) \times e^{-\gamma_w \frac{2M_\phi^2}{v} \frac{1 - v_w}{T_{\text{nuc}}}}. \quad (6)$$

With $\gamma_w(1 - v_w) = \gamma_w - \sqrt{\gamma_w^2 - 1} \rightarrow \frac{1}{2\gamma_w}$ in the limit of fast walls, the density in the plasma frame becomes

$$n_\phi^{\text{BE}} = \frac{T_{\text{nuc}}^3}{24\pi^2} \frac{\lambda^2 v^2}{\pi^2 M_\phi^2} e^{-\frac{M_\phi^2}{v T_{\text{nuc}} \gamma_w}} + \mathcal{O}(1/\gamma_w) \quad . \quad (7)$$

¹Notice the factor of two difference with [18].

The factor $e^{-M_\phi^2/(vT_{\text{nuc}}\gamma_w)}$ is a consequence of $\Theta(p_0 - 2M_\phi^2/v)$ in the the Eq. (5). We can see that in the non-adiabatic limit,

$$\gamma_w > \frac{M_\phi^2}{vT_{\text{nuc}}} \quad , \quad (8)$$

the exponential goes to one and the density becomes independent of the velocity of the wall v_w , as opposed to particle production via dimension five and six operators, as we will see below. The final number density of heavy non-thermal DM, in the unsuppressed region, is of the form

$$n_{\phi}^{\text{BE, PF}} \approx \frac{\lambda^2 v^2 T_{\text{nuc}}^3}{M_\phi^2 24\pi^4} e^{-\frac{M_\phi^2}{vT_{\text{nuc}}\gamma_w}}. \quad (9)$$

After the completion of the PT, the plasma is reheated to some *reheating temperature* T_{reh} , that we can compute in the following way

$$T_{\text{reh}} \approx (1 + \alpha_{\text{nuc}})^{1/4} T_{\text{nuc}} \approx v, \quad \alpha_{\text{nuc}} \equiv \frac{\Delta V}{\rho_{\text{rad}}}, \quad (10)$$

where ΔV is the difference of potential in the broken and the symmetric vacuum.

Dividing by the entropy density after the PT, $s(T_{\text{reh}}) \propto T_{\text{reh}}^3$ and redshifting to today, the final relic abundance today writes

$$\Omega_{\phi, \text{BE}}^{\text{today}} h^2 \approx 2.7 \times 10^5 \times \left(\frac{1}{g_{\star S}(T_{\text{reh}})} \right) \left(\frac{\lambda^2 v}{M_\phi} \right) \left(\frac{v}{\text{GeV}} \right) \left(\frac{T_{\text{nuc}}}{T_{\text{reh}}} \right)^3 e^{-\frac{M_\phi^2}{vT_{\text{nuc}}\gamma_w}}. \quad (11)$$

Here, $g_{\star S}(T)$ is the relativistic degrees of freedom for entropy and we will also use $g_\star(T)$ to indicate the one for the energy. Notice that emitted particles are produced with very large boost factor in the plasma frame

$$\bar{E}_{\phi, \text{plasma}} \approx \frac{1}{2} \frac{\int dx [(p_b^0 + p_c^0)\gamma_w - (p_b^z + p_c^z)v_w\gamma_w]}{\int dx} \sim \frac{1}{2} \frac{M_\phi^2}{T_{\text{nuc}}}. \quad (12)$$

Here, in the last approximation we have used that $p_0^\phi \sim \gamma_w(1 + v_w)T_{\text{nuc}}$, $v_w = \sqrt{1 - \gamma_w^{-2}}$.

The authors in Ref. [22] have shown that in part of the parameter space of the model DM maintains large velocity apart from the usual red-shifting due to the universe expansion and can have a significant *free-streaming* (FS) length L_{FS}

$$L_{\text{FS}} = \int_{z_{\text{eq}}}^{\infty} dz \frac{1}{H} \frac{V_{\text{eq}} \frac{1+z}{1+z_{\text{eq}}}}{\sqrt{\left(V_{\text{eq}} \frac{1+z}{1+z_{\text{eq}}} \right)^2 + 1}}, \quad (13)$$

where we defined $V_{\text{eq}} \equiv V(t_{\text{eq}})$ as the average velocity of the DM at matter-radiation equality and z is the redshift. Observations of small scale structures constrain L_{FS} . The strongest constraint for the DM free-streaming comes from Lyman- α for the DM free-streaming length $L_{\text{FS}} \lesssim 0.059 \text{Mpc}$, which is recast from sterile neutrino mass bound, 5.3 keV [73–75]. This leads to the following bound on the average velocity at matter-radiation equality,

$$V_{\text{eq}} \lesssim 4.2 \times 10^{-5} \quad (\text{Lyman-}\alpha \text{ bound}), \quad (14)$$

Similarly, we can recast the future prospects from 21 centimeters (WDM mass $> 14 \text{keV}$ with the Hydrogen Epoch of Reionization Array [76, 77]), which leads to

$$L_{\text{FS}} < 0.018 \text{ Mpc} \quad \Rightarrow \quad V_{\text{eq}} < 1.2 \times 10^{-5} \quad (21 \text{ centimeters}), \quad (15)$$

and subhalo count (WDM mass $> 18 \text{keV}$ with the Vera Rubin Observatory [78])

$$L_{\text{FS}} < 0.016 \text{ Mpc} \quad \Rightarrow \quad V_{\text{eq}} < 1.0 \times 10^{-5} \quad (\text{subhalo count}). \quad (16)$$

The DM particles which have such non-negligible velocities are denoted in the literature as warm (WDM), with typical velocities

$$V_{\text{eq}}^{\text{WDM}} \sim 10^{-5} \quad . \quad (17)$$

In traditional mechanisms [79] for WDM the candidate mass is generally small, around keV mass scale. However the authors of Ref. [22] have shown that the DM produced in the bubble expansion can also be warm, though very heavy. Indeed starting from equation (12) and assuming that DM is not in kinetic equilibrium with the surrounding plasma we obtain:

$$\begin{aligned} V_{\text{eq}} &\approx \left(\frac{g_{*,s}(T_{\text{eq}})}{g_{*,s}(T_{\text{reh}})} \right)^{1/3} \frac{T_{\text{eq}} p_{\text{DM}}^i}{T_{\text{reh}} M_{\text{DM}}} \sim 0.3 \frac{T_{\text{eq}} p_{\text{DM}}^i}{T_{\text{reh}} M_{\text{DM}}} \\ &\approx 0.3 \frac{T_{\text{eq}} \bar{E}_\phi}{T_{\text{reh}} M_\phi} \approx 10^{-10} \frac{\text{GeV} \times M_\phi}{T_{\text{reh}} T_{\text{nuc}}}, \end{aligned} \quad (18)$$

where T_{eq} is the temperature at matter-radiation equality and T_{reh} , as we will describe more in depth later, the temperature after the completion of the PT. Thus the DM produced in the bubble expansion will be warm if

$$10^5 v T_{\text{nuc}} \sim M_\phi \times \text{GeV}. \quad (19)$$

Very interestingly, this indicates a viable parameter space for explaining the observed abundance of DM being heavy and warm in a range roughly $v \sim \mathcal{O}(100)\text{GeV}$, $M_\phi \sim 10^{(8-9)} \text{GeV}$ and mild supercooling [22]. We now pursue this line of investigation with secluded DM and more realistic DM models. At last we would like to comment on the DM production from the bubble-bubble collisions [15, 26, 80, 81]. This process is always present but is generically subdominant to the DM production *if the non-adiabaticity constraint is satisfied*. As a consequence, we will neglect it in the rest of this study.

3 Production of weakly coupled particles

After the reminder of production via renormalisable operators, we now turn to the production via non-renormalisable operators of the type $h^2 \mathcal{O}_{\text{DS}} / \Lambda^{d-2}$. In this section, we will study the bubble production of dark matter within the framework of weakly coupled theories, where the DM can be a fermion or a dark vector. We also compute the parameter space where it can constitute the total amount of DM, its average velocity and its spectrum at and after the production.

3.1 Production from dimension 5 operator and fermion DM

We start with the case of fermionic DM ψ , which carries conserved quantum number responsible for its stability, coupled to the thermalised sector h via the following non-renormalisable operator

$$\mathcal{L} \supset \frac{h^2 \psi \bar{\psi}}{\Lambda}, \quad (20)$$

where Λ is the UV cutoff and ψ is the fermion DM of mass M_ψ . A very similar procedure to the one presented in the previous section 2 can be followed for the operator in Eq.(20). We show in Appendix A that the probability $P_{h \rightarrow \psi \psi}$ of this splitting is given by

$$P_{h \rightarrow \psi \psi}(p_0) = \frac{v^2}{8\pi^2 \Lambda^2} G(p_0) \Theta(p_0 - 2M_\psi^2 L_w) \Theta(\Lambda^2 - 2p_0 v), \quad (21)$$

where p_0 is the energy of the incoming h in the wall frame. Let us comment on various factors in this equation. The first Θ -function, is an anti-adiabaticity constraint and can be understood in a similar way as the Θ -function in Eq.(4).

When the energy in the center of mass $s_{\text{prod}} \approx 2\gamma_w v T_{\text{nuc}} > \Lambda^2$, the EFT breaks down and we expect the production mechanism to become dependent on the explicit UV completion of the model. For this reason, we will require now that

$$s_{\text{prod}} \approx 2p_0 v \approx 2\gamma_w v T_{\text{nuc}} < \Lambda^2 \quad (\text{EFT validity condition}), \quad (22)$$

as ensured by the second Θ -function of (20). The region that does not meet this condition will be referred to as the *EFT breakdown* region. The $G(p_0)$ is a dimensionless function entering the production process which has the following form

$$G(p_0) \equiv \frac{4}{3} \sqrt{1 - \frac{2M_\psi^2}{p_0 v} \left(\frac{M_\psi^2}{2p_0 v} - 1 \right)} + \log \left[\left| 1 - \frac{p_0 v}{M_\psi^2} - \sqrt{\left(\frac{p_0 v}{M_\psi^2} - 2 \right) \frac{p_0 v}{M_\psi^2}} \right| \right]. \quad (23)$$

After the bubble wall expansion, a non-vanishing abundance of ψ particles has been created. By performing the same analysis as in the renormalisable case, we obtain, in the plasma frame

$$n_\psi^{\text{BE,PF}} \approx g_h \frac{v^2 T_{\text{nuc}}^2 (1 + v_w)}{16\pi^4 \Lambda^2 \gamma_w v_w} \left(2 \frac{M_\psi^2}{v} + \gamma_w T_{\text{nuc}} (2 + v_w - v_w^2) \right) G(\gamma_w T_{\text{nuc}}) e^{-\frac{2M_\psi^2 \gamma_w}{T_{\text{nuc}} v} (1 - v_w)}, \quad (24)$$

leading, if $g_h = 1$, to the DM fraction today:

$$\begin{aligned} \Omega_{\psi, \text{BE}}^{\text{today}} h^2 &\approx 5.38 \times 10^8 \frac{n_\psi^{\text{BE}}}{g_\star^s T_{\text{reh}}^3} \frac{M_\psi}{\text{GeV}} \\ &\approx 5.38 \times 10^8 \frac{1}{g_\star^s} \frac{v^2 T_{\text{nuc}}^3 (1 + v_w)}{16\pi^4 T_{\text{reh}}^3 \Lambda^2 \gamma_w v_w} \left(2 \frac{M_\psi^2}{v T_{\text{nuc}}} + \gamma_w (2 + v_w - v_w^2) \right) G(\gamma_w T_{\text{nuc}}) e^{-\frac{2M_\psi^2 \gamma_w}{T_{\text{nuc}} v} (1 - v_w)}, \end{aligned} \quad (25)$$

which for $v_w \approx 1$ gives finally

$$\Omega_{\psi, \text{BE}}^{\text{today}} h^2 \approx 1.38 \times 10^6 \left(\frac{1}{g_\star^s} \right) \left(\frac{v}{\Lambda} \right)^2 \left(\frac{T_{\text{nuc}}}{T_{\text{reh}}} \right)^3 \left(\frac{M_\psi}{\text{GeV}} \right) \left(\frac{M_\psi^2}{\gamma_w v T_{\text{nuc}}} + 1 \right) G(\gamma_w T_{\text{nuc}}) e^{-\frac{M_\psi^2}{T_{\text{nuc}} v \gamma_w}}. \quad (26)$$

On the top of this production by bubble expansion, there will be a contribution from FI after reheating, computed in Appendix C if $M_\psi \gg T_{\text{reh}}$,

$$\Omega_{\psi, \text{FI}}^{\text{today}} h^2 \approx 5.84 \times 10^4 \left(\frac{M_\psi}{\text{GeV}} \right) \frac{M_{\text{pl}} M_\psi}{g_\star^{3/2} \Lambda^2} \left(\frac{T_{\text{reh}}}{M_\psi} \right)^{3/2} e^{-2M_\psi/T_{\text{reh}}}, \quad (27)$$

which can be sizable if $M_\psi \lesssim 20T_{\text{reh}}$. Here $M_{\text{pl}} \approx 1.2 \times 10^{19}$ GeV is the Planck mass. As a consequence, FI production will be subdominant if

$$\Omega_\psi^{\text{FI}} h^2 \ll 0.1, \quad M_\psi/T_{\text{reh}} > 25 + \log \left(\frac{v}{\Lambda} \frac{M_\psi^2}{v^2} \right), \quad (28)$$

where we approximated $T_{\text{reh}} \sim v$ in the argument of the logarithm.² One finds that in our scenario, the upper bound of the reheating temperature, T_{R} , before the phase transition cannot be too larger

²We also have a contribution of the thermal production before the phase transition. This can be estimated by replacing T_{reh} in Ω_ψ^{FI} with the reheating temperature by inflaton decay, T_{R} , and multiplying an entropy dilution factor $T_{\text{nuc}}^3/T_{\text{reh}}^3$, assuming again that M_ψ is larger than T_{R} . We get

$$\Omega_{\psi, \text{FI}}^{\text{today}} h^2 \approx 5.84 \times 10^4 \left(\frac{M_\psi}{\text{GeV}} \right) \frac{M_{\text{pl}} M_\psi}{g_\star^{3/2} \Lambda^2} \left(\frac{T_{\text{R}}}{M_\psi} \right)^{3/2} \left(\frac{T_{\text{nuc}}}{T_{\text{reh}}} \right)^3 e^{-2M_\psi/T_{\text{R}}} \quad (29)$$

Requiring this to be much smaller than 0.1, we get

$$M_\psi/T_{\text{R}} \gtrsim 20. \quad (30)$$

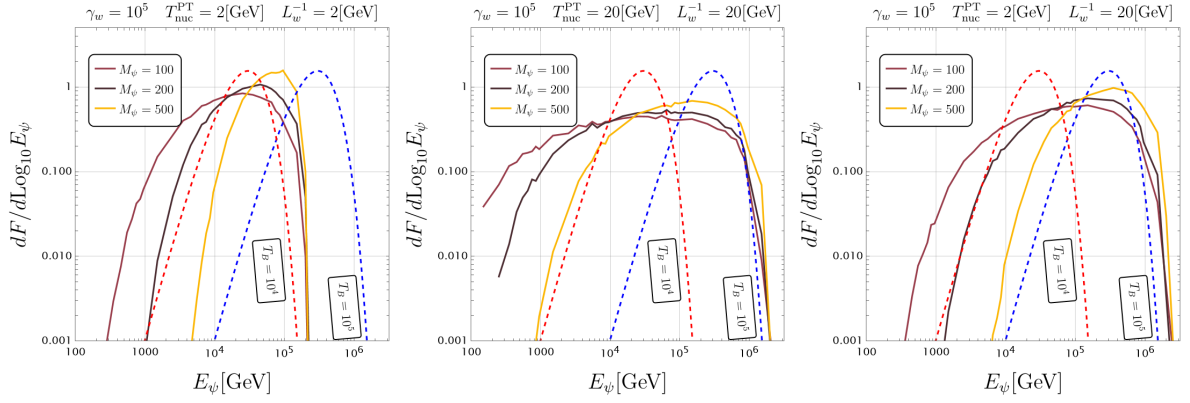


Figure 2: Normalised spectrum of the fermions ψ immediately after emission, via $h \rightarrow \psi\psi$. The thick lines represent the numerical solutions for the spectrum of ψ from bubbles, where E_ψ is the energy in the *plasma frame*. The dashed lines represent the spectrum from a hypothetical thermal Boltzmann abundance of ψ at high temperature ($T_B = 10^4, 10^5$ GeV), which are shown as a comparison for the large E behaviour.

than the upper bound of T_{reh} by the phase transition. Conventionally, we call T_{reh} the reheating temperature after the phase transition, and T_R the temperature of the universe after the reheating due to inflation.

After the DM production, the future of the emitted particles depends on the interactions with the thermal bath, mostly with the h particles, via $\psi h \rightarrow \psi h$. There will be two different regimes that we will now study in detail.

Free-streaming region The first possibility is that the interaction $\psi h \rightarrow \psi h$ is always out of equilibrium after the PT and cannot modify the velocities of DM particles. This is the case when

$$\Gamma_{\psi h \rightarrow \psi h} \sim \frac{T_{\text{reh}}^3}{8\pi^3 \Lambda^2} \ll H(T = T_{\text{reh}}), \quad \frac{T_{\text{reh}} M_{\text{Pl}}}{\Lambda^2} < 1.66 g_*^{1/2} (8\pi^3). \quad (31)$$

Immediately after the phase transition the average energy of the ψ field can be approximated as (see Appendix D for the computation)

$$\bar{E}_{\psi, \text{plasma}} \simeq \frac{L_w^{-1} \gamma_w}{3 \log \frac{\gamma_w T}{M_\psi^2 L_w} - 5.92}. \quad (32)$$

We compare this expression with the energy of the DM for the renormalizable portal in Eq.(12), the dimension-four scalar portal. We observe that the dimension-five case predicts more energetic DM, with the ratio of energies scaling as:

$$\frac{\bar{E}_{\text{dim } 5}}{\bar{E}_{\text{dim } 4}} \sim \frac{\gamma_w T_{\text{nuc}} v}{M_{\text{DM}}^2}. \quad (33)$$

The energy distribution of the DM produced via bubble-plasma collisions will not have the thermal shape immediately after the production. This spectrum can be obtained numerically by convolution of the Boltzmann distribution for the initial particles h with the probability for the heavy-particle production (see details in Appendix D). The results are presented on Fig. 2, where we have used the same normalisation

$$\int_0^\infty dE_\psi \frac{dF}{dE_\psi} = 1, \quad (34)$$

for every curve. Here dF/dE_ψ corresponds to the differential number density and E_ψ is the energy in the plasma frame. At low energies the spectrum starts to rise for $E_\psi \gtrsim M_\psi$, follows a plateau which is finally exponentially cut off by the Boltzmann suppression at $E_\psi \gtrsim \gamma_w L_w^{-1} \sim \gamma_w v^3$.

³Strictly speaking the dark matter is produced during the whole process of the bubble wall expansion, during which

CDM region On the other hand, if the interactions $\psi h \rightarrow \psi h$ are active after the phase transition

$$\frac{T_{\text{reh}} M_{\text{pl}}}{\Lambda^2} > 1.66 g_*^{1/2} (8\pi^3), \quad (35)$$

ψ will quickly slow down until it reaches a kinetic distribution with strongly non-relativistic velocities. DM then becomes usual Cold DM (CDM).

Transition region between CDM and FS. We now address the region between two extreme cases in Eq.(31) and Eq.(35). In order to find the DM velocity V_{eq} in this transition regime, we need to take into account the momentum loss due to rescattering of DM with plasma and follow the average DM energy evolution as a function of T . This effect can be estimated from the following simplified procedure. The momentum of a particle lost in one collision $\psi(p_1)h(p_2) \rightarrow \psi(p_3)h(p_4)$, δp_ψ , is given by [22]

$$\delta p_\psi \approx E_1^\psi - E_3^\psi \approx -t/4T, \quad (36)$$

where the energies are evaluated in the plasma frame and $t \equiv (p_1 - p_3)^2 \approx -2p_1 \cdot p_3$ is the usual Mandelstam variable. Now the equation for the evolution of the ψ average energy \bar{E} , as long as $\bar{E} \approx |p_1| \gg M_\psi$, is

$$a^{-1} \frac{d(\bar{E}a)}{dt} = \langle \sigma_{h\psi \rightarrow h\psi} v_M \rangle \langle \delta p_\psi \rangle_{\text{loss}} n_h, \quad (37)$$

where $\langle \delta p_\psi \rangle_{\text{loss}} \propto \bar{E}$ is the average energy loss in one collision and v_M is the Møller velocity. Using that $d\sigma_{h\psi \rightarrow h\psi}/dt \propto t/s^2 \Lambda^2$, the energy of the collision being approximately $s \approx 4ET$, and neglecting the mass M_ψ for simplicity of the computation, we obtain

$$-\langle \delta p_X \rangle_{\text{loss}}(E) = -\frac{1}{\sigma_{h\psi \rightarrow h\psi}} \int^s dt \frac{d\sigma_{h\psi \rightarrow h\psi}}{dt} \delta p_\psi = \frac{2E}{3}. \quad (38)$$

Then we can rewrite the evolution Eq.(37) as follows

$$\frac{d}{dt} = -HT \frac{d}{dT} \quad \Rightarrow \quad a^{-1} HT \frac{d(a\bar{E})}{dT} = \langle \sigma_{h\psi \rightarrow h\psi} v_M \rangle \bar{E} \frac{2\zeta(3)}{3\pi^2} T^3, \quad (39)$$

where we have assumed that g_* , the relativistic number of d.o.f, is not changing and we used that the number of d.o.f. of the scalar h , $g_h = 1$. The velocity averaged cross-section for the dimension five operator is given by:

$$\langle \sigma_{h\psi \rightarrow h\psi} v_M \rangle = \frac{1}{8\pi\Lambda^2}, \quad (40)$$

where we approximated the relative velocity to be $v_M \approx 2$. And we finally obtain the evolution Eq.(37) in the form

$$\frac{d(a\bar{E})}{a\bar{E}} \approx \frac{1}{12\pi\Lambda^2} \frac{\zeta(3)M_{\text{pl}}}{1.66\pi^2\sqrt{g_*}} dT. \quad (41)$$

The evolution equation can then be trivially integrated to give the final energy of the ψ particle at the decoupling of the scattering

$$\frac{E_f}{E_i} = \left(\frac{T_f}{T_i} \right) \exp \left[-\frac{1}{12\pi\Lambda^2} \frac{2\zeta(3)M_{\text{pl}}}{1.66\pi^2\sqrt{g_*}} (T_i - T_f) \right]. \quad (42)$$

In this expression, the initial temperature T_i is the reheating temperature *after the transition* $T_{\text{reh}} = T_i$. Since this expression was derived using the assumption of relativistic ψ we can use it till the

γ_w is growing. However the DM production will be dominated by the bubbles with the maximal radii just before the collision, thus we believe the corrections will be subleading.

temperature $T_f = T_{\text{NR}}$ when the ψ becomes non-relativistic and $E_\psi \approx M_\psi$. Then after the end of the interactions, the velocity will be simply redshifted by the universe expansion. The velocity at matter-radiation equality is thus given by

$$V_{\text{eq}} = \left(\frac{g_\star(T_{\text{eq}})}{g_\star(T_{\text{NR}})} \right)^{1/3} \frac{T_{\text{eq}}}{T_{\text{NR}}}, \quad \frac{M_\psi}{\bar{E}_\psi} \simeq \frac{T_{\text{NR}}}{T_{\text{reh}}} \exp \left[-\frac{1}{6\pi\Lambda^2} \frac{\zeta(3)M_{\text{pl}}}{1.66\pi^2\sqrt{g_\star}} (T_{\text{reh}} - T_{\text{NR}}) \right]. \quad (43)$$

where \bar{E}_ψ is the average energy given in Eq.(32). The second relation can be solved for T_{NR} and plugged in the first. Combining this with $T_{\text{eq}} \approx 0.8$ eV, we obtain

$$\boxed{V_{\text{eq}} \approx 2 \times 10^{-10} \text{GeV} \times \frac{\bar{E}_\psi}{T_{\text{reh}} M_\psi} \exp \left[-\frac{\zeta(3)}{1.66 \times 6\pi^3 \sqrt{g_\star}} \frac{M_{\text{pl}}(T_{\text{reh}} - T_{\text{NR}})}{\Lambda^2} \right]}. \quad (44)$$

Dynamics of the phase transition and pressure from production We now sketch the dynamics of the PT. Bubbles nucleate generically with a radius

$$R_{\text{nuc}} \propto 1/T_{\text{nuc}}. \quad (45)$$

The expansion of a bubble can proceed in two regimes: either the bubble reaches a steady state motion and the velocity becomes constant (terminal velocity regime), or the bubble keeps accelerating until collision (runaway regime). As long as the pressure from the release of energy is not balanced by the pressure from the plasma, the bubble keeps accelerating with the equation of motion [82, 83]

$$\gamma_w(R) \approx \frac{2R}{3R_{\text{nuc}}} \left(1 - \frac{\Delta\mathcal{P}}{\Delta V} \right) \approx \frac{2R}{3R_{\text{nuc}}}. \quad (46)$$

If the bubble keeps accelerating until collision, the largest velocity is controlled by the radius of the bubble at collision, $\gamma_w^{\text{ter}}(R_\star)$, given by

$$R_\star \approx \frac{(8\pi)^{1/3} v_w}{H[T_{\text{nuc}}]\beta(T_{\text{nuc}})}, \quad \beta(T) = T \frac{d}{dT} \left(\frac{S_3}{T} \right), \quad (47)$$

where R_\star is an estimate for the bubble size at collision and β the inverse dimensionless duration parameter of the transition. We obtain the boost factor at collision

$$\gamma_w^{\text{coll}} \sim \frac{2\sqrt{10}M_{\text{pl}}T_{\text{nuc}}}{\pi^{2/3}\sqrt{8\pi}\sqrt{g_\star}\beta T_{\text{reh}}^2} \approx 0.06 \frac{M_{\text{pl}}T_{\text{nuc}}}{\beta T_{\text{reh}}^2}. \quad (48)$$

However, the pressure from particles coupling to h might terminate the acceleration long before $\gamma_w^{\text{collision}}$ is reached. The study of the bubble wall interaction with the plasma is a field under active investigation [58, 59, 72, 84–104]. In the regimes of ultra-relativistic bubbles, the computation of the terminal velocities [58, 59, 97, 98, 100] amounts to comparing the release of energy ΔV with the plasma pressure in the relativistic regime $\Delta\mathcal{P}(\gamma_w)$. In principle, we could obtain the terminal velocities by solving

$$\Delta V \approx \sum \mathcal{P}(\gamma_w^{\text{ter}}), \quad (49)$$

where $\sum \mathcal{P}(\gamma_w^{\text{ter}})$ is the sum of the different source of pressure.

In the relativistic regime, the computation of the pressure however largely simplifies and the following picture emerges: the pressure is due to the interactions inducing an exchange of momentum from the plasma to the bubble wall. Schematically it reads

$$\mathcal{P}^{\gamma_w \rightarrow \infty} \approx \sum_{ij} \underbrace{\frac{p_z}{p_0} n_i}_{\text{flux}} \times \underbrace{P_{i \rightarrow j}}_{\text{probability } i \rightarrow j} \times \underbrace{\Delta p_{i \rightarrow j}}_{\text{exchange of momentum } i \rightarrow j} \quad (50)$$

where the first factor is the incoming flux of particle species i entering into the wall and having a transition $i \rightarrow j$, i.e. to state j , with an associated loss of momentum $\Delta p_{i \rightarrow j} \equiv p_i - p_j$. This loss of

momentum of the plasma is transmitted to the wall, which is felt by the wall as a pressure. A more complete presentation is provided in Appendix B.

We now investigate the possibility of having runaway walls, as necessary for our production mechanism. The first contribution to the pressure is the pressure from the particles coupling to the BSM Higgses h gaining mass [97],

$$\mathcal{P}_h \approx g_h \frac{m_h^2 T_{\text{nuc}}^2}{24} \quad (\text{BSM Higgs gaining mass: model-independent}), \quad (51)$$

$$\mathcal{P}_i \approx c_i g_i \frac{m_i^2 T_{\text{nuc}}^2}{24} \quad (\text{Particles coupling to } h \text{ gaining mass: model-dependent}), \quad (52)$$

$$\mathcal{P}_{\text{LO}} = \mathcal{P}_h + \sum_i \mathcal{P}_i, \quad (53)$$

where m_h is the mass of the BSM Higgs in the broken phase, $c_i = 1(1/2)$ for bosons(fermions). We assume that this pressure is not enough to prevent to balance the release of energy $\Delta V > \mathcal{P}_{\text{LO}}$. On the other hand, if the BSM Higgs couples sizably with gauge coupling g to gauge bosons, the emission of soft transverse gauge bosons [58, 98] and longitudinal gauge bosons [100], would induce a pressure

$$\mathcal{P}_g \propto \frac{g^3}{16\pi^2} \gamma_w T_{\text{nuc}}^3 v \quad (\text{emission of soft bosons: model-dependent}), \quad (54)$$

preventing runaway. The intuitive picture in Eq.(50) permits to understand how the pressure on the wall can increase with the energy $\gamma_w T$ without ever threatening unitarity: in the wall frame, $n_i \propto \gamma_w T^3$ while $\Delta p_z \sim v$ and the plasma frame $n_i \propto T^3$ while $\Delta p_z \sim \gamma_w v$. In both frames, the probability of the emission of the soft gauge boson is bounded $P_{\phi \rightarrow \phi A} \ll 1$.

We thus assume that the BSM Higgs does not couple to gauge bosons so that $\mathcal{P}_g \rightarrow 0$ [60] or the gauge coupling is small, e.g., $g \lesssim 0.01 \beta^{1/3} \left(\frac{v}{10^{10} \text{GeV}}\right)^{1/3}$ by taking $T_{\text{reh}} \sim T_{\text{nuc}} \sim (\Delta V)^{1/4} \sim v$ and assuming Eq.(54) for the friction, and in this case, the pressure from gauge boson emission remains always subleading. We finally focus on the unavoidable (model independent) pressure induced by the production. Indeed, the transition $h \rightarrow \psi\psi$ has a non-vanishing exchange of momentum, which is transmitted to the wall at the production. Because of this, the wall undergoes a plasma pressure [59] (see Appendix B for the details of the computation)

$$\Delta \mathcal{P}_{h \rightarrow \psi\psi}^{\text{prod}} \approx \frac{1}{8\pi^2} \frac{v^3 n_h \gamma_w}{\Lambda^2} \quad (\text{production pressure: model-independent}), \quad (55)$$

which we call the *production pressure* [59] and could in principle stop the wall acceleration. Let us insist on the fact that the maximal pressure that can be induced in the *context of the EFT validity* is given by

$$\gamma_w^{\text{max}} \approx \frac{\Lambda^2}{2vT_{\text{nuc}}} \quad \Rightarrow \quad \mathcal{P}_{h \rightarrow \psi\psi}^{\text{prod}} \Big|_{\text{max}} \approx g_h \frac{v^2 T_{\text{nuc}}^2}{16\pi^4}, \quad (56)$$

where we set $2\gamma_w v T_{\text{nuc}} = \Lambda^2$. This remains in principle always smaller than the pressure from the h obtaining a mass in Eq.(51). We can thus safely neglect it.

At the end of the day, the boost factor involved in the production of DM is given by

$$\gamma_w^{\text{max}} = \text{Min}[\gamma_w^{\text{ter}}, \gamma_w^{\text{coll}}]. \quad (57)$$

The value of γ_w^{ter} strongly relies on the physics of the PT sector, namely the presence of gauge bosons and further particles, as well as the amount of supercooling. Following the discussion above, we however consider the following situation

$$\Delta V > \mathcal{P}_h \gg \mathcal{P}_{h \rightarrow \psi\psi}^{\text{prod}} \Big|_{\text{max}}, \quad \mathcal{P}_g \sim 0 \quad \Rightarrow \quad \text{Runaway regime} \quad (58)$$

As a consequence, in the remainder of this paper we will always take $\gamma_w^{\text{max}} = \gamma_w^{\text{coll}}$ from Eq.(48).

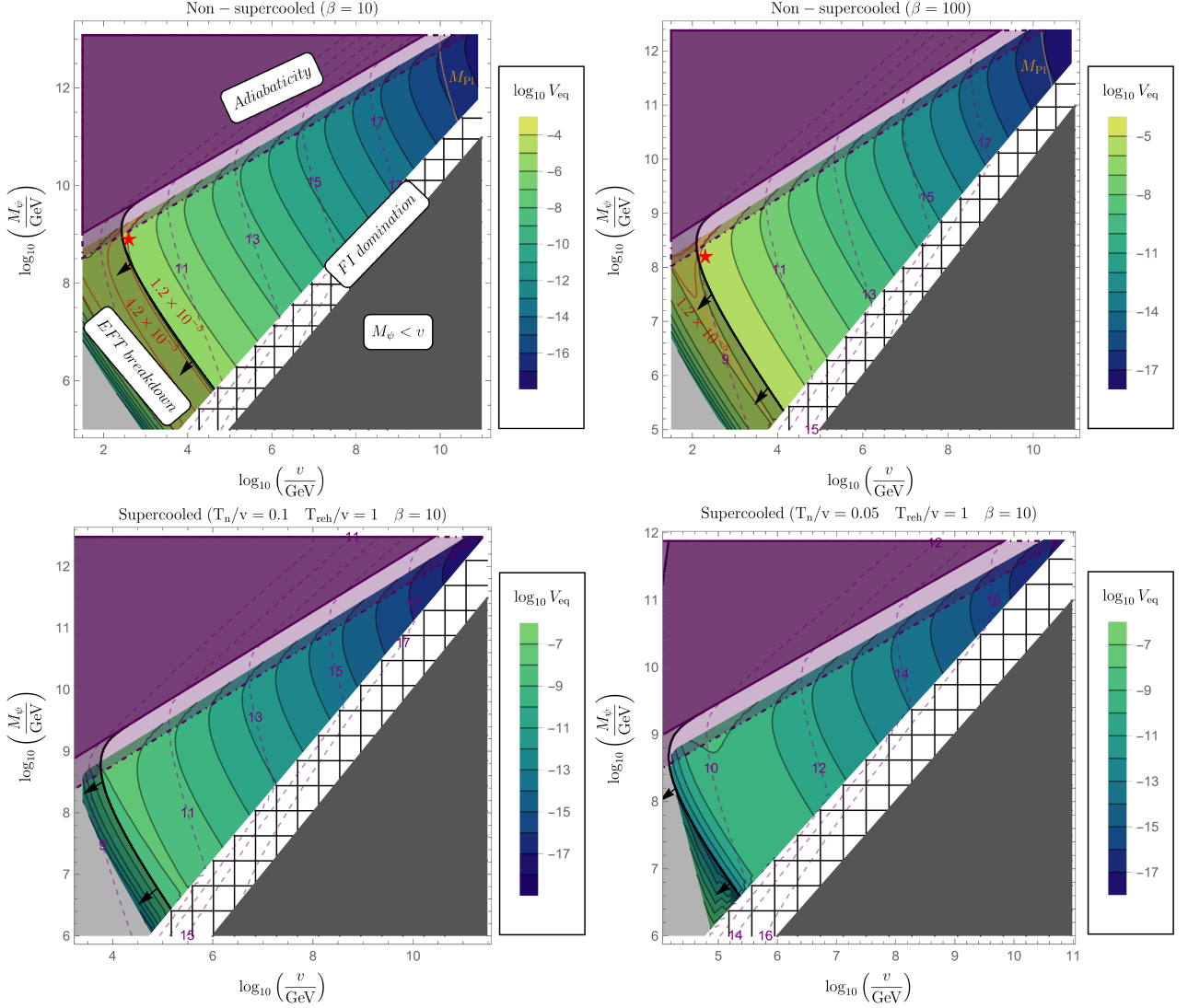


Figure 3: Contour plots of $\log_{10}(V_{\text{eq}})$ for the operator $\frac{h^2 \bar{\psi} \psi}{\Lambda}$ and for various values of β and T_{nuc} , while $T_{\text{reh}} = v$. Purple dashed lines indicate the isocontours of the UV cutoff, $\log_{10}\left(\frac{\Lambda}{\text{GeV}}\right)$. The shaded area to the left of the solid black line excludes the region where the EFT analysis breaks down, i.e. $2\gamma v T_{\text{nuc}} > \Lambda^2$. The dark gray region in the lower right of each plot indicates $v > M_\psi$. The dark purple area indicates the region where the anti-adiabaticity condition is not satisfied $\gamma_w T v \leq 2M_\psi^2$. The light purple area denotes the region defined by the conditions $M_\psi^2 \in \gamma_w T_{\text{nuc}} v \times [0.05, 0.5]$, in this region DM can be produced, but expression in Eq.(32) is not valid. In the white hatched regions, FI is the dominant process for DM production. The red lines represent the current and future experimental bounds on the velocity, as given by Eqs. (14, 15), and the red star marks the specific points we study in the main text. Light grey area in the lower right corner of the plot indicates the DM in the thermal equilibrium.

Results and discussion After describing the dynamics of the phase transition, we now put it all together and study the parameter space. In principle, we have five parameters in our model

$$\left(\gamma_w, \alpha_{\text{nuc}}^{1/4} \approx \frac{T_{\text{nuc}}}{v}, v, \Lambda, M_\psi \right), \quad (59)$$

but for the plots we fix the value of T_{nuc}/v and set $\gamma_w = \gamma_w^{\text{max}} = \gamma^{\text{coll}}(\beta, T_{\text{nuc}}, T_{\text{reh}})$ to the value at bubble collision (48). We take $T_{\text{reh}} = v = T_{\text{nuc}}$ for the non-supercooled case. The value of Λ is obtained by requiring that the produced DM abundance, given by Eq.(26) and Eq.(27);

$$\Omega_{\psi, \text{today}} h^2 = \Omega_{\psi, \text{BE}}^{\text{today}} h^2 + \Omega_{\psi, \text{FI}}^{\text{today}} h^2, \quad (60)$$

matches the observation of DM in the universe today. Thus we are left just with two free parameters v - scale of the phase transition and M_ψ dark matter mass, which we use for plotting. In Fig. 3 we present several versions of this plot for the various values of β and T_{nuc}/v . We observe that the DM can be fairly warm for $v_\phi \in [10^2, 10^5]$ GeV, close to the EFT breakdown. We observe an ankle in the Λ contours, followed by an exponential suppression. This change of behaviour can be understood from Eq.(26) where we set $\Omega_{\psi, \text{BE}}^{\text{today}} h^2 = 0.12$ and solve for Λ . When the DM production becomes exponentially suppressed, the Λ drops exponentially to compensate, creating an ankle in the Λ contours. We note that generically thermal DM is incompatible with EFT (light grey regions in the bottom-left corner of the plot). More specifically, this region was obtained by solving the right expression of Eq. (43) for T_{NR} and checking if the DM particle is in equilibrium or not at this temperature. Note that the naive condition of (35) leads almost to the same contour.

At last we present two benchmark points with very heavy and warm DM:

- $\beta = 10$:

$$\begin{aligned} v &= 400 \text{ GeV}, & M_\psi &= 8 \times 10^8 \text{ GeV} \\ \Lambda &= 6.3 \times 10^9 \text{ GeV}, & \gamma_w &= 1.7 \times 10^{14}, & V_{\text{eq}} &= 9.5 \times 10^{-6}. \end{aligned} \quad (61)$$

- $\beta = 100$:

$$\begin{aligned} v &= 200 \text{ GeV}, & M_\psi &= 1.6 \times 10^8 \text{ GeV} \\ \Lambda &= 1.5 \times 10^9 \text{ GeV}, & \gamma_w &= 3.4 \times 10^{13}, & V_{\text{eq}} &= 7.1 \times 10^{-6}. \end{aligned} \quad (62)$$

These points are represented on Fig. 3 by a red star and might be soon observable by structure formation probes like Lyman- α and 21 cm [76, 77] or sub-halo count [78]. As we will also comment in section 5, such points would also likely produce a copious gravitational wave signal that might be detectable with the space interferometer LISA.

3.2 Production from dimension 6 operator and vector DM

We can now go through the same steps for the dark vector DM produced via a dimension 6 operator of the form

$$\frac{h^2 F_{\mu\nu} F^{\mu\nu}}{\Lambda^2}, \quad (63)$$

where $F_{\mu\nu}$ is the field strength of a dark vector γ . The probability of the production of transverse gauge bosons is again computed in Appendix A and reads⁴

$$P_{h \rightarrow \gamma\gamma} \equiv P_{h \rightarrow \gamma^\pm \gamma^\mp} \approx \frac{v^3 p_0}{\Lambda^4} \frac{1}{4\pi^2} \Theta(p_0 v - 2M_\gamma^2). \quad (64)$$

⁴Longitudinal mode production, on the other hand, is model dependent. If we consider the mass of the vector obtained from Higgsing, then one can go back to section 2 for the production of longitudinal modes by considering that ϕ is the BSM Higgs field for the vector's mass. When the mass of the Higgs and the vector are both light, according to the equivalence theorem (whose validity was discussed in [26]), the estimation is the same as the Higgs case. Since the BSM Higgs gets a VEV, it decays but the vector boson does not need to decay because of the unbroken dark charge conjugation symmetry: $\phi \rightarrow \phi^*$, $F \rightarrow -F$.

One might be worried that the probability of the interaction increases with the energy and threaten the unitarity when $p_0 \gg \Lambda^4/v^3$. However, we expect the EFT description to break down around $p_0 \sim \Lambda^2/v$, and the UV description to unitarize the theory.

The abundance produced by bubble expansion is then given by

$$n_\gamma^{\text{BE,PF}} \approx g_h \frac{2\gamma_w v^3 T_{\text{nuc}}^4}{(\pi\Lambda)^4} e^{-\frac{M_\gamma^2}{T_{\text{nuc}} v \gamma_w}}. \quad (65)$$

Hence, with $g_h = 1$, the vector DM fraction today is of the form

$$\Omega_{\gamma,\text{today}}^{\text{BE}} h^2 \approx 1.1 \times 10^7 \times \left(\frac{1}{g_\star(T_{\text{reh}})} \right) \left(\frac{\gamma_w v^2 T_{\text{nuc}} M_\gamma}{\Lambda^4} \right) \left(\frac{v}{\text{GeV}} \right) \left(\frac{T_{\text{nuc}}}{T_{\text{reh}}} \right)^3 e^{-\frac{M_\gamma^2}{v T_{\text{nuc}} \gamma_w}}. \quad (66)$$

As for the fermion production, an unavoidable FI contribution comes from the reheating temperature after the transition, and is given by (see Appendix C for the complete computation)

$$\Omega_{\gamma,\text{today}}^{\text{FI}} h^2 \approx \begin{cases} 8.76 \times 10^4 \left(\frac{M_\gamma}{\text{GeV}} \right) \frac{M_{\text{pl}} M_\gamma^3}{g_\star^{3/2} \Lambda^4} \sqrt{\frac{M_\gamma}{T_{\text{reh}}}} e^{-2M_\gamma/T_{\text{reh}}} & \text{when } T_{\text{reh}} \ll M_\gamma \\ 1.05 \times 10^6 \left(\frac{M_\gamma}{\text{GeV}} \right) \frac{M_{\text{pl}} T_{\text{reh}}^3}{g_\star^{3/2} \Lambda^4} & \text{when } T_{\text{reh}} \gg M_\gamma \end{cases}. \quad (67)$$

The total abundance is then given by

$$\Omega_{\gamma,\text{today}}^{\text{tot}} h^2 = \Omega_{\gamma,\text{today}}^{\text{BE}} h^2 + \Omega_{\gamma,\text{today}}^{\text{FI}} h^2. \quad (68)$$

If the mass of the vector boson is below the reheating temperature, $M_\gamma < T_{\text{reh}}$, the FI is relativistic, then the ratio of the relic abundances will be

$$\frac{\Omega_{\text{BE}}}{\Omega_{\text{FI}}} \simeq 10^2 \left(\frac{\gamma_w T_{\text{nuc}}}{M_{\text{pl}}} \right) \left(\frac{v}{T_{\text{reh}}} \right)^3 \left(\frac{T_{\text{nuc}}}{T_{\text{reh}}} \right)^3 \approx \frac{6}{\beta} \left(\frac{T_{\text{nuc}}}{T_{\text{reh}}} \right)^6. \quad (69)$$

Here, we have taken into account only FI after the PT and in the second equality we considered the maximal terminal velocity given by Eq.(48).⁵ With $\beta \sim 10$, we observe that $\frac{\Omega_{\text{BE}}}{\Omega_{\text{FI}}}$ is most likely to be smaller than one and we hence conclude that in the case of relativistic FI, the BE contribution will be typically subdominant. For this reason we will impose $M_\gamma > v$ in our future computations.

The conclusion about the pressure from production is the same as in the dimension five case: The pressure on the bubble wall is given by

$$\mathcal{P}_{h \rightarrow \gamma\gamma} \approx n_h \frac{v^4}{\Lambda^4} \frac{\gamma_w^2 T}{2\pi^2} \quad (\text{production pressure}). \quad (72)$$

Following the same reasoning as for the dimension five case, the maximal pressure within the EFT validity regime is

$$\mathcal{P}_{h \rightarrow \gamma\gamma}^{\text{prod}} \Big|_{\text{max}} \approx g_h \frac{v^2 T_{\text{nuc}}^2}{32\pi^4}, \quad (73)$$

where we set $2\gamma_w v T_{\text{nuc}} = \Lambda^2$. This remains in principle always smaller than ΔV and the LO pressure from the ϕ obtaining a mass. We can thus safely neglect it. Immediately after the production, the

⁵Generically, assuming FI also happened before the immediately after inflation, at T_R , we have the further contribution

$$\Omega_{\gamma,\text{today}}^{\text{FI}} h^2 \approx 8.76 \times 10^4 \left(\frac{M_\gamma}{\text{GeV}} \right) \frac{M_{\text{pl}} M_\gamma^3}{g_\star^{3/2} \Lambda^4} \sqrt{\frac{M_\gamma}{T_R}} \left(\frac{T_{\text{nuc}}}{T_{\text{reh}}} \right)^3 e^{-2M_\gamma/T_R}, \quad (70)$$

which again requires

$$M_\gamma \gtrsim 20T_R. \quad (71)$$

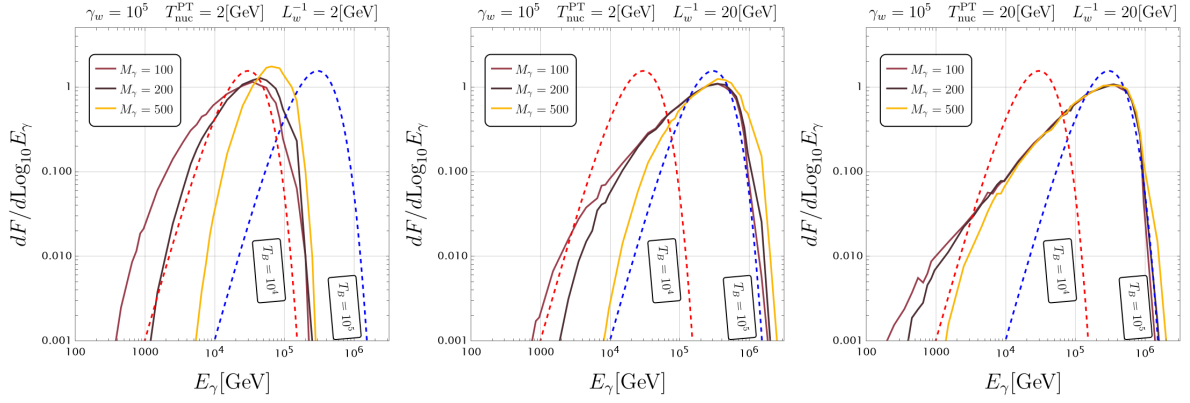


Figure 4: Normalised spectrum of the vector DM γ immediately after emission via $h \rightarrow \gamma\gamma$. Same as Fig.2, but now for the dimension six operator.

average energy in the plasma frame of the produced vectors is given by (see Appendix D for the numerical and the analytical computation.)

$$\bar{E}_\gamma \approx C_\gamma \gamma_w L_w^{-1}, \quad C_\gamma \approx 0.16. \quad (74)$$

As for the fermions, the spectrum of the vectors immediately after production is not a thermal spectrum. We present the details of the computation of the spectrum in Appendix D and show it for some values of the parameters in Fig.4. The spectrum, compared to the spectrum of the dimension five case presented in Fig.2, does not show a plateau, but an increasing slope until the Boltzmann exponential tail. As for the dimension five, at low energies the spectrum starts to rise for $E_\gamma \gtrsim M_\gamma$.

As before, after production, the vector DM can rescatter via $\gamma h \rightarrow \gamma h$, inducing an energy loss that we can compute. The only difference is the energy dependence of the cross-section $\langle \sigma v \rangle \propto \frac{T\bar{E}}{\Lambda^4}$:

$$\frac{d(a\bar{E})}{a\bar{E}^2} = \frac{\zeta(3)}{16\pi^3 1.66\sqrt{g_\star}} \frac{M_{\text{pl}}}{\Lambda^4} T dT. \quad (75)$$

Then solving for the energy we get the following relations

$$V_{\text{eq}} = \left(\frac{g_\star(T_{\text{eq}})}{g_\star(T_{\text{reh}})} \right)^{1/3} \frac{T_{\text{eq}}}{T_{\text{NR}}} \quad M_\gamma \simeq \frac{T_{\text{NR}}}{T_{\text{reh}}} C_\gamma \gamma_w v \left[1 + \frac{\zeta(3)}{16\pi^3 1.66\sqrt{g_\star}} \frac{M_{\text{pl}} \gamma_w v T_{\text{reh}}^2}{\Lambda^4} \right]^{-1}, \quad (76)$$

which combines to the following expression for the velocity at equality

$$V_{\text{eq}} = \left(\frac{g_\star(T_{\text{eq}})}{g_\star(T_{\text{reh}})} \right)^{1/3} \frac{T_{\text{eq}}}{M_\gamma} \frac{C_\gamma \gamma_w v}{T_{\text{reh}}} \left[1 + \frac{\zeta(3)}{16\pi^3 1.66\sqrt{g_\star}} \frac{M_{\text{pl}} \gamma_w v T_{\text{reh}}^2}{\Lambda^4} \right]^{-1}, \quad (77)$$

giving

$$V_{\text{eq}} \approx 0.32 \times 10^{-10} \frac{\text{GeV} \times \gamma_w v}{T_{\text{reh}} M_\gamma} \left[1 + \frac{\zeta(3)}{16\pi^3 1.66\sqrt{g_\star}} \frac{M_{\text{pl}} \gamma_w v T_{\text{reh}}^2}{\Lambda^4} \right]^{-1}. \quad (78)$$

We present results on the Fig. 5, following exactly the same conventions of the Fig. 3. The cut-off scale is fixed in order to reproduced the DM abundance and the boost factor γ_w is fixed to be the one at collision (48). The color scheme for the plots is exactly the same as in Fig. 3. We observe that we can get WDM with velocities $V_{\text{eq}} \sim (0.5 - 1) \times 10^{-4}$.

We now discuss the differences and similarities between the fermion and the vector production.

3.3 Comparison between the dimension five and the dimension six production

Let us now comment on the differences between the production of fermions and that of vector particles. First, looking at Fig. 2 and Fig. 4, we observe that the initial spectrum have different energy

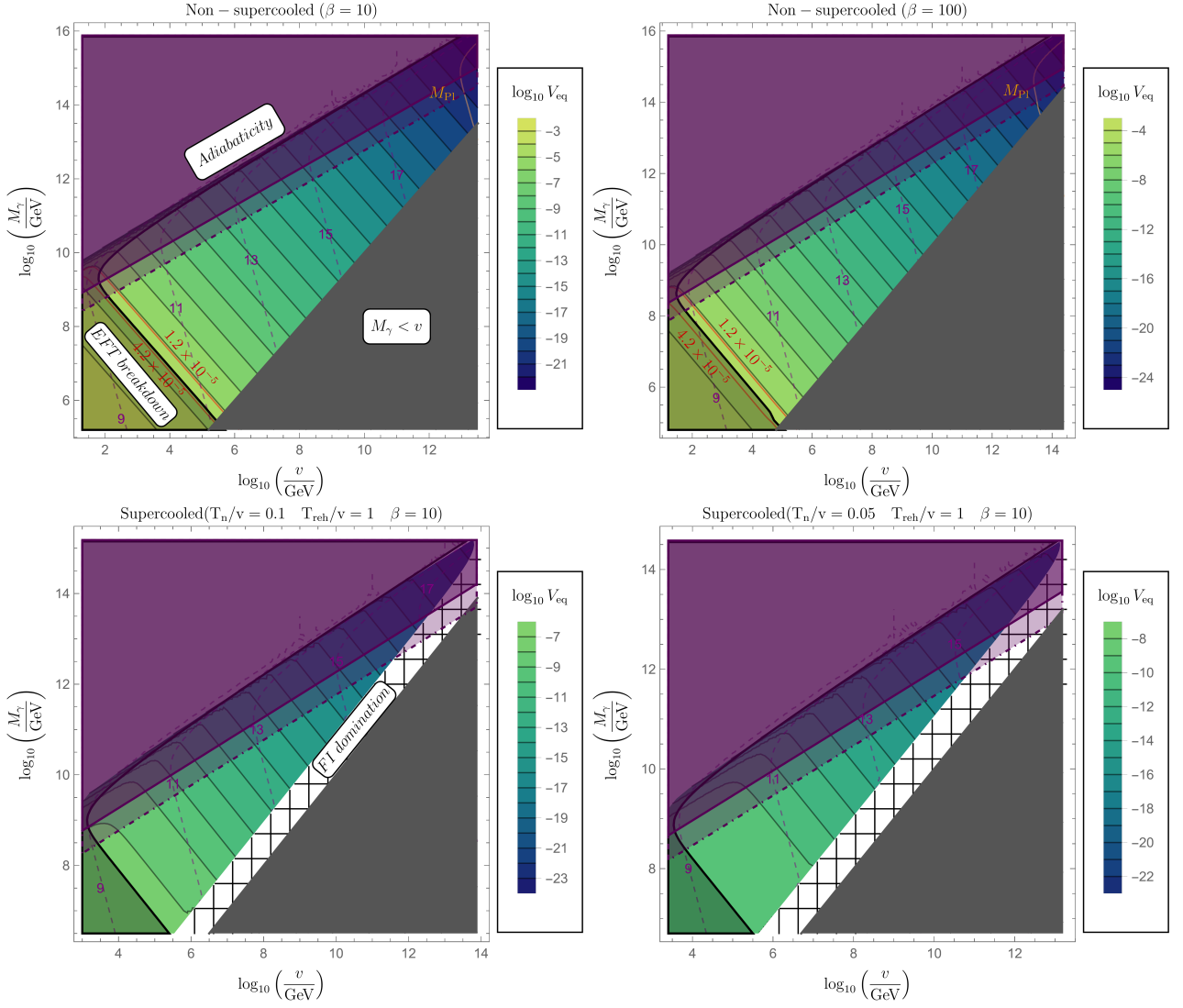


Figure 5: Contour plots of $\log_{10}[V_{\text{eq}}]$ for the operator $\frac{h^2 FF}{\Lambda^2}$ for different β , T_{nuc} and $T_{\text{reh}} \sim v$. Coloring scheme and various contours are exactly the same as in the Fig.3

dependences:

$$(\text{fermion}): \frac{dF_\psi}{dE_\psi} \propto E_\psi^0, \quad (\text{vector}): \frac{dF_\gamma}{dE_\gamma} \propto E_\gamma^1, \quad (79)$$

in between the Boltzmann suppressed regime and the rise at small E .

Secondly, in both the fermion and the vector case, the EFT validity constraint, requires that the DM is generically *free-streaming* after the production and does not thermalise efficiently. Interestingly we find that the parameter space with $V_{\text{eq}} \sim 10^{-5}$ is much larger in dimension six models compared to the dimension five. For the vector emission, the DM is warm in a larger band near the EFT breaking bound. A third observation is that there is no striking difference in the parameter space (Λ, M) allowing the dark sector to contain the total amount of observed DM. This is because the ratio of the production of vector over fermions scales like

$$\frac{n_{\text{BE}}^\gamma}{n_{\text{BE}}^\psi} \propto \mathcal{O}(0.1) \frac{\gamma_w^{\text{coll}} T_{\text{nuc}} v}{\Lambda^2}, \quad (80)$$

up to logarithmic corrections. The consequence is that the very large γ_w^{coll} partially cancel the large suppression from $T_{\text{nuc}} v / \Lambda^2$. A similar cancellation does not occur for the FI, where we have

$$\frac{n_{\text{FI}}^\gamma}{n_{\text{FI}}^\psi} \propto \frac{M_{\text{DM}}^2}{\Lambda^2}, \quad (81)$$

and, as we consider $M_{\text{DM}} \ll \Lambda$, the FI contribution is less relevant. As a consequence, for both cases, a phase transition at the EW scale *can* produce the total amount of observed DM and than this DM will be typically warm. In this case, h may be a BSM Higgs field relevant to the electroweak phase transition.

Finally, we find that in both cases we can match the observed DM abundance by taking $\Lambda \sim M_{\text{pl}}$, $v = 10^{10-14} \text{GeV}$. This is a particularly interesting observation because i) we expect on general grounds any dark sector to be coupled to the thermal sector by at least Planck-suppressed operators, ii) The PT of the scale of $v = 10^{10-14} \text{GeV}$ agrees with the seesaw and Peccei-Quinn scales and happens in various well-motivated models for the neutrino mass or the strong CP problem [61–65, 67–69]. In those models, ultra-relativistic bubble walls can populate the dark sector particles coupled to the visible sector solely via gravity, and explain the DM abundance. In this scenario, the GW signal features a peak frequency of 10^{2-6}Hz in addition to the scale-invariant one from cosmic strings, since the models spontaneously break $U(1)$ global/gauge symmetry.

4 Production of strongly coupled gluons

In this section, we study the case in which the dark sector is a strongly coupled pure Yang-Mills theory, which means that the considered dark sector is purely made of gluons in the deconfined phase or glueballs in the confined phase (for the review see [105–107]). We will thus explore the phenomenology of bubble wall produced gluons which later hadronize and account for the DM in the universe.

4.1 Glueballs as WIMP dark matter

If we assume that the dark sector is controlled by a pure Yang-Mills theory, the glueball DM does not behave as a WIMP, which annihilates to reduce the comoving number efficiently. The difference is that, since a pion does not exist in the pure Yang-Mills theory, the glueball is the lightest particle of the DS. The glueballs decrease their number density via the $3 \rightarrow 2$ process of the glueball self-interaction, while the glueballs in the final state are more energetic, transforming the number density into thermal energy. This makes the scenario different from usual freeze-out. On top of this, glueball DM has several interesting properties: first, the glueball can only have higher dimensional interactions with other particles that are not charged under $SU(N)$. As a consequence, for glueball DM, the stability

can be easily satisfied without imposing any further symmetry. Second, glueballs have an irreducible self-interaction rate controlled by the confinement scale. This self-interaction may be relevant to the small-scale problem or, more recently called galaxy diversity problem, stating that the rotation curves for spiral galaxies have inner slopes in a diverse range [108–110]. Very interestingly, the self-interactions of glueballs might also make the SMBH [111] grow faster.

4.2 The set-up

We now turn to the mechanism for the population of the dark glueball sector. Assuming a vanishing initial glueball abundance, again, there will be two mechanisms that lead to the population of the dark sector, being FI and BE. Both processes will occur via the following effective operator that couples the strong dark sector $G^{\mu\nu}$ with the thermal sector h , which could be the Higgs or another scalar field in the thermal bath that undergoes the phase transition,

$$\frac{h^2 G_{\mu\nu} G^{\mu\nu}}{\Lambda^2}. \quad (82)$$

This effective coupling will produce gluons via the scattering $hh \rightarrow gg$ for the FI production case and via the splitting $h \rightarrow gg$ by bubble expansion.⁶

For the FI, as well as for the BE, the strongly coupled sector can be populated in two different ways. The production mechanism can directly produce thermalised gluons or glueballs. Moreover, as the glueballs are not naturally protected by a symmetry, they will have a natural decay channel to a pair of h via the dimension six operator. In this case, the decay rate is too large to explain the dark matter stability. To avoid this fast decay,⁷ we require that $m_h \sim v > M_G \sim 5\Lambda_{\text{conf}}$ [113], so that the glueballs cannot directly decay to h . Other decay products involve the SM particles and arise from dimension six operators, and we will discuss this possibility later in this section.

4.3 Comparison of the FI and the BE in two regimes

In this section, we estimate the relative abundance from FI and from bubble production, within the two regimes of interest: first, the deconfined gluon phase is never attained during the evolution. In this situation, *glueballs are generated directly*. As we will see below, we anticipate that the FI contribution predominates over the bubble production in this regime. Secondly, *a gluon plasma* forms after the thermalization of the dark sector. We will discuss the conditions necessary for this transition in the following sections.

1. Glueball regime In this regime, the gluons will hadronize immediately to N_{part} free-streaming glueballs. As a consequence, the abundance of glueballs immediately *after* FI can be obtained following the same computation as for the vector production in Eq.(164) and multiplying by the multiplicity factor N_{part} ⁸ and the color factor $N^2 - 1$. We obtain

$$Y_G^{\text{FI}} \approx \frac{45(N^2 - 1)M_{\text{pl}} T_{\text{reh}}^3}{3.32g_\star^{3/2} \pi^7 \Lambda^4} N_{\text{part}}(T_{\text{reh}}/\Lambda_{\text{conf}}), \quad (83)$$

where the FI production occurs *after* the phase transition. For the case of BE production, one obtains

$$Y_G^{\text{BE}} \approx (N^2 - 1) \frac{\gamma_w v^3 T_{\text{nuc}}}{\pi^6 g_\star \Lambda^4} \left(\frac{T_{\text{nuc}}}{T_{\text{reh}}} \right)^3 N_{\text{part}}(\gamma_w T_{\text{reh}}/\Lambda_{\text{conf}}), \quad (84)$$

⁶The gravitational freeze-in production via a purely Planck-suppressed operator was presented in [112].

⁷An alternative possibility is to consider a parity conserving dark sector, i.e., the strong CP phase is zero. Then the lightest parity odd glueball gets more stabilized and can behave as dark matter. This also predicts decaying DM because the parity symmetry is explicitly broken in the standard model sector, and the decay rate of the parity odd glueball is not absolutely zero but suppressed compared with the parity even one. We do not consider this possibility in this paper, because the parity odd one is usually not the lightest dark particle, and it would annihilate into the parity even ones. The annihilation channels also exist, making the discussion more complicated.

⁸The multiplicity factor takes into account large number of hadrons(glueballs) produced and grows with energy. Using [114] for pure gluonic theory we find $N_{\text{part}} \propto \exp \sqrt{\frac{2C_A}{\pi b} \log \frac{s}{\Lambda^2}} \sim \exp \sqrt{\frac{24}{11} \log \frac{s}{\Lambda^2}}$

which we extracted from Eq.(65), and multiplied again by the multiplicity and color factor. The ratio of those two production mechanisms is given by

$$\frac{Y_G^{\text{BE}}}{Y_G^{\text{FI}}} \approx \frac{3.32\pi g_\star^{1/2} \gamma_w v^3 T_{\text{nuc}}}{45 M_{\text{pl}} T_{\text{reh}}^3} \left(\frac{T_{\text{nuc}}}{T_{\text{reh}}} \right)^3 N_{\text{part}}(\gamma_w) \approx 2.4 \frac{\gamma_w T_{\text{nuc}}}{M_{\text{pl}}} \left(\frac{T_{\text{nuc}}}{T_{\text{reh}}} \right)^3 N_{\text{part}}(\gamma_w), \quad (85)$$

which is bounded by above

$$\frac{Y_G^{\text{BE}}}{Y_G^{\text{FI}}} \lesssim \frac{1}{\beta} \left(\frac{T_{\text{nuc}}}{T_{\text{reh}}} \right)^5 N_{\text{part}}(\gamma_w), \quad (86)$$

where we assumed that $T_{\text{reh}} \approx v$ and we substituted the value of the terminal velocity given in Eq.(48). Since we expect $\beta \gtrsim 10$, we estimate that in the case of direct glueball emission, the FI mechanism is most likely dominating, or at least at the same order of magnitude compared to bubble production. We will thus leave this regime aside in the remainder of the discussion and leave it to further studies.

2. Gluon regime Interestingly, strongly coupled theories can potentially lead to very different DM scenarios compared to a weakly interacting DS. Namely, if the energy transfer from the phase transition field to the strongly coupled sector proves sufficiently efficient, it leads to the formation of a gluon plasma. For this reason, determining the total energy transfer is of paramount importance in order to ascertain if a gluon plasma will be formed. Moreover, the initial energy density of the strong sector will also control the final DM abundance. This is because the $gg \rightarrow ggg$ interaction transforms the initially high-energetic gluon to multiple lower energetic gluons. Hence, the final number of glueballs depends on the initial energy, governing the final DM abundance. We will therefore now proceed to present the expressions for the energy density of both mechanisms.

The average energy of an emitted gluon produced by BE is similar to the case of dark vectors and reads:

$$\bar{E}_g \approx C_g \gamma_w L_w^{-1} \sim C_g \gamma_w v. \quad (87)$$

where C_g is expected to be similar to C_γ , defined in Appendix D, and therefore $C_g \approx C_\gamma \approx 0.16$. To obtain the energy density deposited in the gluon sector, the above expression has to be multiplied by the number density given by Eq. (65). Moreover, the energy density of the dark sector immediately after FI has been already computed in Appendix C. The energy densities by BE and FI are hence given by

$$\rho_{\text{BE}} \sim n_g \bar{E}_g \approx (N^2 - 1) C_g \frac{2\gamma_w^2 v^4 T_{\text{nuc}}^4}{(\pi\Lambda)^4}, \quad \rho_{\text{FI}} \approx 10.2 \frac{(N^2 - 1) T_{\text{reh}}^7 M_{\text{pl}}}{\sqrt{g_\star} \pi^5 \Lambda^4}, \quad (88)$$

respectively. Notice the quadratic dependence on the boost factor γ_w for the case of BE production. This can be understood in the following way: the energy density is given by $E_g n_g$ where both quantities, n_g and \bar{E}_g are Lorentz boosted and scale like $\gamma_w \gg 1$. Of course, similar to the weakly coupled cases, a condition for the validity of our computation of the BE-produced abundance is that the EFT is still valid for large values of γ_w that are considered, i.e.

$$\Lambda^2 > s \approx 2\gamma_w v T_{\text{nuc}} \quad (\text{breakdown of the EFT}). \quad (89)$$

These expressions allow for a straightforward comparison

$$\frac{\rho_{\text{BE}}}{\rho_{\text{FI}}} \approx C_g \frac{2\pi\gamma_w^2 v^4 T_{\text{nuc}}^4}{T_{\text{reh}}^7 M_{\text{pl}}} \sim 2\pi C_g \frac{\gamma_w^2 T_{\text{nuc}}^4}{v^3 M_{\text{pl}}} \sim 0.02 C_g \frac{M_{\text{pl}}}{\beta^2 v} \left(\frac{T_{\text{nuc}}}{v} \right)^6, \quad (90)$$

where we used Eq. (48) in the last step. We notice a very large enhancement due to the factor M_{pl}/v , which makes the BE production largely dominant if the cooling is mild. We however notice that if the cooling is strong $T_{\text{nuc}} \ll 10^{-2}v$, then it is unlikely that the BE mechanism can dominate. As the case of mild cooling appears to be more interesting phenomenologically, we will focus on it from now on.

Lastly, we would like to comment on the glueball production in the bubble-bubble collisions, similar to the processes described in Ref. [15, 26, 80, 81]. Unlike in weakly coupled theories, energy transfer to the dark sector will be more efficient, as the glueballs will have energy $\sim \gamma v$. However, the parameter space where EFT description is valid is much smaller for the bubble-bubble collisions compared to plasma-bubble case. That said, the importance of the bubble-bubble collisions remains an open question and we leave the analysis of this process for the future studies.

4.4 Conditions for the formation of a gluon plasma

We have observed that if the dark sector reaches a gluon plasma, the BE mechanism is likely to dominate over the associated FI contribution for non-supercooled PTs. We can wonder now: what are the conditions to reach such gluon plasma state after the phase transition? We find two conditions:

- First, one should transfer sufficient energy to the dark sector

$$\rho_g \approx C_g(N^2 - 1) \frac{2\gamma_w^2 v^4 T_{\text{nuc}}^4}{(\pi\Lambda)^4} > \Lambda_{\text{conf}}^4. \quad (91)$$

- Second, even if the energy transfer to the dark sector is large enough, but the initial density of glueballs is very small, a gluon plasma will not be formed. To estimate the minimal necessary density, we require that the scattering rate of glueballs is larger than the Hubble expansion rate:

$$\Gamma_{GG \rightarrow GG} \sim \Gamma_{GGG\dots} > H \quad (\text{Thermalisation of the dark sector}), \quad (92)$$

where the rate $\Gamma_{GGG\dots}$ is the total rate of the processes in which three or more glueballs are produced in GG collisions. It would scale parametrically the same as $\Gamma_{GG \rightarrow GG}$. We can estimate this rate as follows:

$$\Gamma_{GGG\dots}^{\text{BE}} \sim n_G^{\text{BE}} \times \sigma_{GGG\dots} \approx \sigma_{GGG\dots} \times C_g(N^2 - 1) \frac{2\gamma_w v^3 T_{\text{nuc}}^4}{(\pi\Lambda)^4} N_{\text{part}} \left(\frac{\gamma_w v}{\Lambda_{\text{conf}}} \right) \quad (93)$$

where we have used Eq.(65) $n_G \approx N_{\text{part}} n_\gamma \approx N_{\text{part}} \frac{2\gamma_w v^3 T_{\text{nuc}}^4}{(\pi\Lambda)^4}$. The scattering amongst glueballs can be estimated by naive dimensional analysis. The estimate for the cross section of $2 \rightarrow 3$ processes then reads [107]

$$\sigma_{GGG\dots} \sim \sigma_{GG \rightarrow GG} \sim \frac{(4\pi)^3}{N^2 \Lambda_{\text{conf}}^2} \sim \frac{220}{\Lambda_{\text{conf}}^2} \left(\frac{3}{N} \right)^2, \quad (94)$$

which is similar to the observed total QCD cross section $\sigma_{\text{QCD}} \sim \frac{250}{\text{GeV}^2}$ [115]. If this condition is fulfilled, the interaction $GG \rightarrow GGG$ (or more glueballs in the final state) is active and the number density of glueballs starts to grow very quickly leading to the formation of the gluon plasma. Note that the composite glueball has a cross-section of $\sim 1/\Lambda_{\text{conf}}^2$ even at the high energy collision, similarly to the nucleon scattering.

So far, we only considered collisions between fast glueballs produced via BE. However a fast glueball produced via BE could have a collision with a slow glueball produced via FI. In this setting, there are always two populations of glueballs: 1) some cold and slow glueballs coming from FI and 2) some very boosted glueballs produced by the bubble. Population 1) will naturally serve as targets for the fast and scarce glueballs of population 2) to induce $GG \rightarrow GGG\dots$ interactions. If this process is efficient it will also lead to the rapid increase of the glueball density and the formation of the quark gluon plasma. The scattering rate can be estimated as

$$\Gamma_{GGG\dots}^{\text{FI}} \sim n_G^{\text{FI}} \sigma_{GGG\dots} \approx 220 \left(\frac{3}{N} \right)^2 \frac{2(N^2 - 1) T_{\text{reh}}^6 M_{\text{pl}}}{3.32 g_\star^{1/2} \pi^5 \Lambda^4 \Lambda_{\text{conf}}^2} \approx 0.4 \frac{v^6 M_{\text{pl}}}{\Lambda^4 \Lambda_{\text{conf}}^2}. \quad (95)$$

In what follows, we will take

$$\Gamma_{GGG\dots} = \Gamma_{GGG\dots}^{\text{FI}} + \Gamma_{GGG\dots}^{\text{BE}} > H. \quad (96)$$

as a sufficient condition for the rapid increase of the gluon number density. Thus, we will use the conditions in Eq.(91) and Eq.(96) as a criteria for the dark sector being in the deconfined phase. This naive picture will be modified if the following processes, possibly relevant for the thermalisation, are active $hG \rightarrow hG$, $hG \rightarrow hGG$ and $GG \rightarrow hh$. The rate of those interactions is roughly

$$\begin{aligned} \Gamma_{hG \rightarrow hGG} &\sim \Gamma_{hG \rightarrow hG} \approx \frac{n_h \bar{E}_g T_{\text{reh}}}{8\pi\Lambda^4} \sim C_g \frac{\gamma_w T_{\text{reh}}^4 v}{8\pi^3 \Lambda^4}, \\ \Gamma_{GG \rightarrow hh} &\sim n_G \frac{\gamma_w v}{8\pi\Lambda^4}. \end{aligned} \quad (97)$$

However those effects are only relevant if only

$$H < \Gamma_{GG \rightarrow hh} \quad H < \Gamma_{hG \rightarrow hGG}, \quad (98)$$

but the viable space of parameters of our mode requires $\Lambda_{\text{conf}} \ll v$. As we will confirm below, we find that this effect is never relevant. Moreover, in all the parameter space where $\Gamma_{GG \rightarrow hh}$ might be active, the rate for thermalization of the dark sector $\Gamma_{GG \rightarrow GGG}$ is much larger and lead to a gluon plasma before energy might be given back to the thermal sector. We can then always neglect it.

We now turn to the abundance of the glueball DM today.

4.5 The abundance of Glueball DM today

We here restrict to the region of the parameter space where the gluon plasma is reached after thermalisation. In this case, the produced glueballs interact with each other and melt to a thermalized gluon plasma soon after the production around the cosmic temperature $T = T_{\text{reh}}$. The process is as follows: the energetic dark gluons produced by the BE form glueballs because, at production, gluons are initially underdense compared to Λ_{conf}^3 . Then, due to scattering, the typical energy of each glueball gradually decreases while the total number of glueballs increases. When the number density of glueballs becomes higher than $\sim \Lambda_{\text{conf}}^3$, the glueball picture no longer holds and we get a dark gluon plasma. The number density continues to increase (see Ref. [116] for the detailed thermalization in the $\Lambda_{\text{conf}} \rightarrow 0$ limit.) until the system reaches thermal equilibrium. We consider that this thermalization completes within $O(1)$ Hubble time because of the nature of the strong interaction. Then the whole gluon sector will be characterized just by the corresponding temperature T_g . The interaction between these gluons with temperature T_g ($\ll T_{\text{SM}}$, i.e. the temperature of the SM sector, which is also the temperature for the BSM Higgs h) and the thermal sector h is negligible due to the nature of the higher dimensional interaction, and we call the gluon sector, the dark sector. Afterwards, due to the expansion of the universe, T_g as well as T_{SM} redshifts. When T_g becomes smaller than Λ_{conf} , the glueballs are formed again due to the confinement phase transition, for which we assume that the entropy production is negligible.

The calculation of the glueball relic abundance proceeds in a standard way [105–107] and in our discussion we will follow closely the notations of [117]. Then introducing the parameter

$$B \equiv \frac{T_g^4}{T_{\text{SM}}^4} = \frac{g_* \rho_g}{2(N^2 - 1)\rho_{\text{SM}}} = \frac{30\rho_g}{2\pi^2(N^2 - 1)T_{\text{SM}}^4} = \frac{30C_g}{\pi^6} \frac{\gamma_w^2 v^4}{\Lambda^4} \left(\frac{T_{\text{nuc}}}{T_{\text{reh}}} \right)^4, \quad (99)$$

so that the relic abundance of glueball DM today is given by

$$\frac{(\Omega h^2)_G}{(\Omega h^2)_{\text{DM}}} \approx 0.056(N^2 - 1) \left(\frac{B}{10^{-12}} \right)^{3/4} \left(\frac{\Lambda_{\text{conf}}}{\text{GeV}} \right) W \left[2.1 \frac{N^2 - 1}{N^{18/5}} B^{3/10} \left(\frac{M_{\text{pl}}}{\Lambda_{\text{conf}}} \right)^{3/5} \right]^{-1}, \quad (100)$$

where the function W is the inverse function of xe^x . The value of Λ allowing to match the observed abundance of DM can be approximately found by taking the $W \sim 1$, and we obtain

$$\Lambda_{\text{observed DM}} \approx 10 \left(\frac{M_G}{\text{GeV}} \right)^{1/3} \left(\frac{v T_{\text{nuc}}}{T_{\text{reh}}^2} \right) \left(\frac{M_{\text{pl}} T_{\text{nuc}}}{\beta} \right)^{1/2} \rightarrow 10 \left(\frac{M_G}{\text{GeV}} \right)^{1/3} \left(\frac{M_{\text{pl}} v}{\beta} \right)^{1/2}, \quad (101)$$

where the last limit is the case of the non-supercooling. We however use the exact expression in the plots.

4.6 The production during the EWPT

It is particularly interesting to consider the case in which the h field, producing the gluonic sector, is actually the Higgs field. Although this is not the case for the previous vector field and fermion case, the glueballs are produced differently. In the context of the EWPT, assuming it is a first order PT it has been shown in Ref. [58] that the pressure from the heavy gauge bosons, W^\pm and Z , on the bubble wall prevents the EWPT from realistically having highly relativistic boost factors. It was shown that γ_w scales like $(v/T_{\text{nuc}})^3$ [23], hence, ultra-relativistic speeds are reached at the price of a long supercooling of the EWPT.

Using the estimate in Eq.(90), we find

$$\left. \frac{\rho^{\text{BE}}}{\rho^{\text{FI}}} \right|_{\text{EWPT}} \approx 2\pi C_g \frac{\gamma_{\text{EWPT}}^2 T_{\text{nuc}}^4}{v_{\text{EW}}^3 M_{\text{pl}}} \propto \frac{v_{\text{EW}}}{M_{\text{pl}}} \left(\frac{T_{\text{nuc}}}{v_{\text{EW}}} \right)^{-2} \ll 1. \quad (102)$$

From those estimates, we can conclude that during the EWPT, the production of the dark gluon sector via BE is far too subdominant and can be discarded.

4.7 Phenomenological constraints on glueball DM

In the subsection, we discuss the constraints that exist on glueball DM. They come mainly from the decays of DM and from the strong interactions of glueballs amongst each other.

4.7.1 Bullet cluster bounds on the scattering rate

We can estimate the scattering rate among glueballs by

$$\sigma_{GG \rightarrow GG} \sim \frac{220}{\Lambda_{\text{conf}}^2} \left(\frac{3}{N} \right)^2. \quad (103)$$

The bound from the bullet cluster is estimated to be [118, 119]

$$\frac{\sigma_{GG \rightarrow GG}}{M_G} \lesssim 2 \times 10^3 \text{GeV}^{-3} \quad \Rightarrow \quad \frac{1}{\Lambda_{\text{conf}}^3} \lesssim 50 \text{GeV}^{-3}, \quad (104)$$

where we assumed that $M_G \sim 5\Lambda_{\text{conf}}$ [113]. We thus can conclude that

$$\Lambda_{\text{conf}} \gtrsim 0.25 \text{ GeV}. \quad (105)$$

4.7.2 Decay of the glueball

The glueball can decay via different channels depending on its mass. If $\Lambda_{\text{conf}} > v$, then the glueballs decay very fast to h . So we require that $\Lambda_{\text{conf}} < v$. We will consider the constraint on the decay of G to the SM particles, because it is usually more stringent than the decay into some additional dark light particles.

When $M_G < v_{EW}$. We first focus on the decay to a SM fermion pair. For the reasons advocated in section 4.6, matching the observed DM abundance requires that h is a BSM Higgs. This BSM Higgs can however always share a quartic portal with the SM, which cannot be forbidden by symmetries. Denoting the physical Higgs with a capital letter H and the BSM Higgs with a lower case h , we can have

$$\lambda|H|^2h^2, \quad (106)$$

like in [23] and the effective operator controlling the decay is then given by

$$\mathcal{L}_{\text{eff}} \supset \frac{\lambda v_{EW} v}{m_h^2 m_H^2} \frac{v}{\Lambda^2} y_f \bar{f} f G_{\mu\nu} G^{\mu\nu}, \quad (107)$$

because the mixing term is $\lambda H^2 h^2 \supset 2\lambda v_{EW} v H h$. Thus h couples to the SM fermions via mixing with the Higgs boson $y_e \frac{\lambda v_{EW} v}{m_h^2}$. Taking into account that $m_h \sim v$ and $m_H \sim v_{EW}$, the decay rate becomes

$$\Gamma_{G \rightarrow f^+ f^-} \sim \lambda^2 \frac{y_f^2 M_G^7}{\Lambda^4 v_{EW}^2} \quad t_{G,\text{decay}} \sim \frac{10^{23} s}{y_f^2 \lambda^2} \left(\frac{\Lambda}{10^9 \text{ GeV}} \right)^4 \left(\frac{0.1 \text{ GeV}}{M_G} \right)^7. \quad (108)$$

The decay is most dominant via the heaviest fermion pair available, i.e. $M_G > 2m_f = 2y_f v_{EW}$.

When $M_G > v_{EW}$. In the case of $M_G > 2m_H$, the glueballs can decay to a pair of Higgses via the operator

$$\mathcal{L}_{\text{eff}} \supset \lambda \frac{v^2}{m_h^2} \frac{H H G_{\mu\nu} G^{\mu\nu}}{\Lambda^2}, \quad (109)$$

which is much less suppressed. The decay rate becomes

$$\Gamma_{G \rightarrow H H} \sim \lambda^2 \frac{M_G^5}{\Lambda^4} \quad t_{G,\text{decay}} \sim \frac{10^2 s}{\lambda^2} \left(\frac{\Lambda}{10^9 \text{ GeV}} \right)^4 \left(\frac{100 \text{ GeV}}{M_G} \right)^5. \quad (110)$$

The bounds on the lifetime of DM impose $t_{G,\text{decay}} \sim 10^{26-27} s$, e.g., [120]. Taking the estimate for $\Lambda_{\text{observed DM}}$ in Eq.(101), we obtain an estimate for the decay time, in the limit of non-supercooling

$$t_{G,\text{decay}} \sim \frac{10^{11} s}{\lambda^2 \beta^2} \left(\frac{100 \text{ GeV}}{M_G} \right)^{11/3} \left(\frac{v}{\text{GeV}} \right)^2. \quad (111)$$

In Fig. 6, we present the region of parameter space allowing to match the observed abundance of DM from bubble expansion assuming the melted regime. On the Left panel, the black (full, dashed and dash-dotted) lines show the region matching the observed abundance of DM (or a fraction of it in dashed lines), in the melted regime. We shade all the regions where our computation is not valid: the yellow region excludes the region where the EFT is broken, according to Eq.(89), the orange region shows the region where the $hG \rightarrow hG$ interaction is *active*, according to Eq.(97), and the red region is the region where $hh \rightarrow GG$ is active. Those reactions would couple the thermal sector to the glueball sector and induce an unacceptably large abundance of glueballs. Finally, the blue region shows the region where the interaction $GG \rightarrow GG\dots$ is *inactive* according to Eq.(96) with the rates for FI and BE given by Eq.(95) and (92), respectively, and the gray region denotes the region where the requirements of having enough energy to form a gluon plasma is not fulfilled, i.e. Eq.(91). In the latter two regions, we do not expect the dark sector to ever reach a deconfined gluon phase and then our computation is likely not valid.

On the Right panel of Fig.6, we observe that successful glueball DM can occur in a vast region of the parameter space

$$v \in [10^4, 10^{15}] \text{ GeV}, \quad \Lambda \in [10^{13}, 10^{19}] \text{ GeV}, \quad \Lambda_{\text{conf}} \in [0.25, 5 \times 10^6] \text{ GeV}. \quad (112)$$

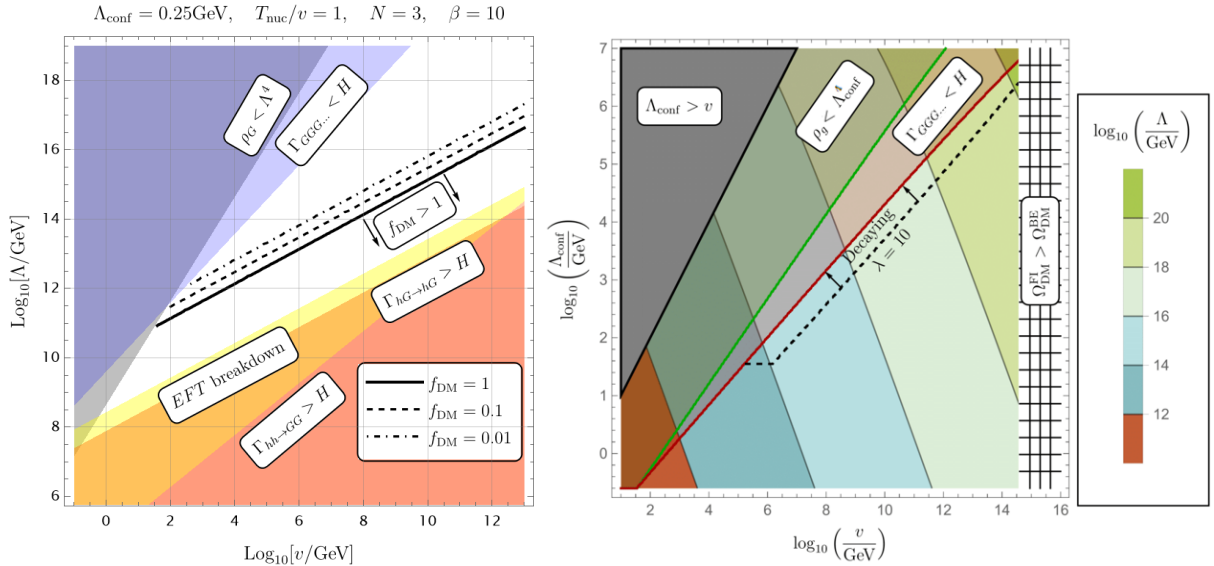


Figure 6: **Left:** We show the different conditions in the specific example $\Lambda_{\text{conf}} = 0.25 \text{ GeV}$. The full black line satisfies the two conditions in $\rho_g > \Lambda_{\text{conf}}^4$ and $\Gamma_{GGG\dots} > H$ and match the observed abundance while the dashed line only underproduce DM for $f_{\text{DM}} \equiv \Omega_G^{\text{BE}}/\Omega_{\text{DM,obs}} = [0.1, 0.01]$. **Right:** Parameter space allowing to match the observed abundance of DM with the bubble production. When $\Gamma_{GGG\dots} \ll H$, the glueballs are free-streaming, as in the previous discussion for dark vector field. This could contribute to the dark radiation. In the dashed black contour, we present the region of DM that would have decayed by today if $\lambda = 10$.

For almost all the range of the strongly coupled sector that matches the DM abundance, the DM is stable on cosmological timescales. However in a thin band of the parameter space, for large glueball masses, and for a large portal coupling $\lambda \approx 10$, the DM is decaying.

At the other edge of the parameter space, for light glueballs, the strong interactions among DM glueballs can show up in bullet cluster-like events if $\Lambda_{\text{conf}} \sim 0.3 \text{ GeV}$, hence we use this value as a lower limit for the range of the parameter scan.

5 GW signal from Dark Matter production

In the previous sections we studied the production of DM during the phase transition. We saw that it required runaway walls and rather slow transitions with moderate values of β . In turn this specific type of phase transition is expected to induce a large background of gravitational waves due to the sound waves and the collision of bubble walls, making this mechanism possibly detectable via GW interferometers.

In this section, we quickly comment on this GW background. In the simplest version of our model, the energy of the phase transition goes to the bubble wall stress, the shells of produced DM and strongly boosted fluid shells. For such a fast bubble expansion the bulk flow model [121]⁹ is expected to describe the stochastic GW background the best [60] and we use it to assess the current and future experimental sensitivities. We present the signal of the GW signal induced together with the integrated power-law sensitivities of LISA, LIGO, CE, ET, MAGIS, BBO in Fig.7. Following Ref. [121] the GW signal, assuming $v_w \rightarrow 1$, takes the form

$$h^2 \Omega_{\text{GW}} = h^2 \Omega_{\text{peak}} S(f, f_{\text{peak}}) \quad S(f, f_{\text{peak}}) = \frac{(a+b) f_{\text{peak}}^b f^a}{b f_{\text{peak}}^{(a+b)} + a f^{(a+b)}}, \quad (a, b) \approx (0.9, 2.1), \quad (113)$$

⁹The authors thank Jorinde Van De Vis and Ryusuke Jinno for helpful discussions on the bulk flow model.

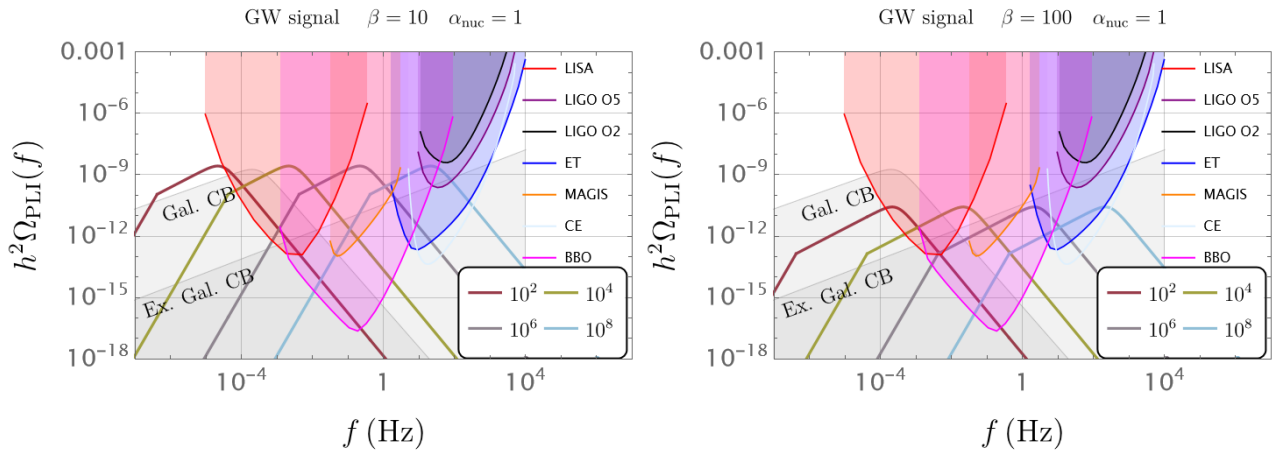


Figure 7: Shape of the GW signal for the model producing DM with $\alpha_{\text{nuc}} = 1$ and $\beta = 10$ (Left) and $\beta = 100$ (Right) for different values of $v = 10^2, 10^4, 10^6, 10^8$ GeV. The signal-to-noise ratio and the sensitivity curves can be build following the recommendations of [126–133]. The gray regions are the expected foregrounds from galactic and extra-galactic compact binaries that we obtain from the recommendations in [134–136].

with

$$\begin{aligned}
 h^2 \Omega_{\text{peak}} &\approx 1.06 \times 10^{-6} \left(\frac{H}{\beta} \right)^2 \left(\frac{\alpha_{\text{nuc}} \kappa}{1 + \alpha_{\text{nuc}}} \right)^2 \left(\frac{100}{g_\star} \right)^{1/3} & \text{and} & \quad \kappa = 1, \\
 f_{\text{peak}} &\approx 2.12 \times 10^{-3} \left(\frac{\beta}{H_{\text{reh}}} \right) \left(\frac{T_{\text{reh}}}{100 \text{ GeV}} \right) \left(\frac{100}{g_\star} \right)^{-1/6} & \text{mHz}. & \quad (114)
 \end{aligned}$$

Note that on the top of this spectrum, one needs to impose an IR cut-off required by causality for $f < H_{\text{reh}}/2\pi$.

The complicated problem of the separation of the unavoidable astrophysical background (from time to time called *foreground*) from the possible cosmological background is still under vivid investigation [122–125]. As a consequence, we shade in gray the regions where we expect a strong foreground from galactic and extra-galactic compact binaries. This foreground is still subject to very large uncertainties and will depend on our abilities to resolve individual sources, it should therefore be interpreted with caution.

6 Summary and conclusions

In this paper, we have studied the bubble wall production of DM in a secluded sector connected to the thermal bath by a non-renormalisable portal. We have first systematically studied the abundance of DM, the spectrum of the emitted DM and its evolution for a dimension five (fermion) and a dimension six portal (vector) weakly coupled DM scenarios. Unfortunately, both scenarios are incompatible with EW phase transition, since the bubble expansion will not be sufficiently fast due to the gauge boson friction. Requiring that the BE production matches the observable abundance, we observe that very interestingly a phase transition at scale close to the EW scale, $v \sim 10^2 - 10^3$ GeV, can lead to DM masses up to 10^{10} GeV. We observed that in both cases, of vector and fermion production, the EFT validity constraint requires that the DM is generically *free-streaming* after the production. On the other hand, both the dimension five and the dimension six operators allow in a band of the parameter space the production of WDM with $V_{\text{eq}} \sim 10^{-5}$ or slightly faster. We found that in the instance of an electroweak scale PT, on top of the expected GW signal accompanying the strong PT, the bubble wall production of secluded warm fermionic and vector DM will be WDM and have of large mass of order $M_{(\psi, \gamma)} \sim 10^8 - 10^9$ GeV. This is for example illustrated by the red star on Fig.3. Those signatures constitute a striking smoking gun of our scenario.

In parallel, we have calculated the pressure on the bubble wall caused by higher dimensional operators. Reassuringly, this new contribution to the pressure remains minor across all the parameter spaces we examined, making it unlikely to significantly alter the velocity of the wall.

We also studied the case of a pure Yang-Mills confining dark sector, where the DM is composed of dark glueballs. In this scenario, we focused on the production of a thermal dark gluon plasma. Here, the energy of each individual boosted glueball, initially produced by the wall, contributes to increasing the final number density of glueballs through the self-interactions of the dark sector. Consequently, glueball DM is always slow. The formation of a gluon plasma, combined with the Bullet Cluster constraint on DM self-interactions, requires the mass of the glueball to be within the range of $[0.25, 5 \times 10^6]$ GeV.

Finally, we emphasize that our proposal for DM production is inherently accompanied by strong signals in the stochastic GW background. This makes our proposal highly detectable.

Acknowledgements

It is a pleasure to thank Iason Baldes for comments on the manuscript. XN is supported by the iBOF “Un-locking the Dark Universe with Gravitational Wave Observations: from Quantum Optics to Quantum Gravity” of the Vlaamse Interuniversitaire Raad and the ”Strategic Research Program High-Energy Physics of the Vrije Universiteit Brussel”. MV is supported by the “Excellence of Science - EOS” - be.h project n.30820817, and by the Strategic Research Program High-Energy Physics of the Vrije Universiteit Brussel. WY is supported by JSPS KAKENHI Grant Nos. 20H05851, 21K20364, 22K14029, 22H01215, and 23K22486. AA is supported in part by the MUR projects 2017L5W2PT. AA also acknowledges support by the European Union - NextGenerationEU, in the framework of the PRIN Project “Charting unexplored avenues in Dark Matter” (20224JR28W).

A Bubble-Plasma production probability

In this appendix, we gather the details of the computation of the production via Bubble-Plasma interactions that we have studied in the main text.

A.1 Dimension five operator

In the main text, we studied the impact of the following dimension 5 operator

$$\frac{h^2\psi\bar{\psi}}{\Lambda}, \quad (115)$$

where Λ is the UV cutoff, h undergoes the phase transition $h \rightarrow h + v$ and ψ is a fermion of mass M_ψ . We present the details of the computation of the probability of $h \rightarrow \psi\psi$ production. The kinematics of the process can be parameterized as follows

$$\begin{aligned} p_a &= (p_0, 0, 0, p_0), \\ p_b &= ((1-x)p_0, k_\perp, 0, \sqrt{(1-x)^2 p_0^2 - M_\psi^2 - k_\perp^2}), \\ p_c &= (xp_0, -k_\perp, 0, \sqrt{x^2 p_0^2 - M_\psi^2 - k_\perp^2}), \end{aligned} \quad (116)$$

where $M_\psi < \Lambda$ is the mass of the ψ which is constant. From this point we can thus introduce a WKB wave for the outgoing particles X, as presented in [58] and reviewed in [59]. Our computation is typically valid in the wall frame for very large velocities: $p_z \sim \gamma_w T_{\text{nuc}} \gg 1/L_w$. Within this WKB approach, the matrix element takes the form

$$\mathcal{M} = i \left(\frac{V_s}{A_s} - \frac{V_h}{A_h} \right), \quad (117)$$

where the $s(h)$ subscript denotes the symmetric(higgsed) side. So

$$A \equiv p_0 - \sqrt{(1-x)^2 p_0^2 - M_\psi^2 - k_\perp^2} - \sqrt{x^2 p_0^2 - M_\psi^2 - k_\perp^2}. \quad (118)$$

and the squared vertex $|V_{h \rightarrow \psi\psi}^s|^2 = 0$ and¹⁰

$$\begin{aligned} |V_{h \rightarrow \psi\psi}^h|^2 &= 4 \frac{v^2}{\Lambda^2} (p_b \cdot p_c - M_\psi^2) \\ &= 4 \frac{v^2}{\Lambda^2} \left(p_0^2 x(1-x) - p_0^2 x(1-x) \sqrt{1 - \frac{M_\psi^2 + k_\perp^2}{p_0^2 x^2}} \sqrt{1 - \frac{M_\psi^2 + k_\perp^2}{p_0^2 (1-x)^2}} + k_\perp^2 - M_\psi^2 \right) \\ &= 2 \frac{v^2}{\Lambda^2} \frac{1}{x(1-x)} (M_\psi^2 (2x-1)^2 + k_\perp^2). \end{aligned} \quad (119)$$

Expanding for $x^2(1-x)^2 p_0^2 \gg k_\perp^2 + M_\psi^2$, we obtain

$$A_h = A_s \approx \frac{M_\psi^2 + k_\perp^2}{2p_0(1-x)x}. \quad (120)$$

The amplitude matrix then becomes

$$|\mathcal{M}_{h \rightarrow \psi\bar{\psi}}|^2 = 8 \frac{v^2}{\Lambda^2} \left(\frac{p_0}{M_\psi} \right)^2 \frac{x(1-x)}{1 + \left(\frac{k_\perp}{M_\psi} \right)^2} \left(1 - \frac{4x(1-x)}{1 + \left(\frac{k_\perp}{M_\psi} \right)^2} \right). \quad (121)$$

The value of k_\perp^{\max} can be straightforwardly extracted from the non-adiabaticity condition. For more details on how to recover this conditions from basic principles, see Appendix A of [18] and Appendix H of [72] for further discussions. Therefore, the upper boundary of the k_\perp integral reads:

$$\frac{M_\psi^2 + k_\perp^2}{2vp_0} < (1-x)x \quad (\text{non-adiabaticity condition}). \quad (122)$$

which implies that the upper bound on the integral is given by

$$(k_\perp^{\max})^2 = 2vp_0x(1-x) - M_\psi^2 \approx 2vp_0x(1-x). \quad (123)$$

Using the matrix element in Eq.(121) and the boundaries in Eq.(123) and integrating over the phase space, the probability of producing $h \rightarrow \psi\psi$ is

$$\begin{aligned} P_{h \rightarrow \psi\psi} &\approx \frac{1}{8p_0^2} \int_{b_+}^{b_-} \frac{dx}{x(1-x)} \int_0^{2p_0vx(1-x) - M_\psi^2} \frac{dk_\perp^2}{8\pi^2} |\mathcal{M}_{h \rightarrow \psi\bar{\psi}}|^2 \\ &\approx \frac{v^2}{8\pi^2 \Lambda^2} \left[\frac{4}{3} \sqrt{1 - \frac{2M_\psi^2}{p_0v}} \left(\frac{M_\psi^2}{2p_0v} - 1 \right) + \log \left(\left| 1 - \frac{p_0v}{M_\psi^2} - \sqrt{\left(\frac{p_0v}{M_\psi^2} - 2 \right) \frac{p_0v}{M_\psi^2}} \right| \right) \right]. \end{aligned} \quad (124)$$

and we defined

$$b_+ \equiv \frac{1 - \sqrt{1 - \frac{2M_\psi^2}{p_0v}}}{2}, \quad b_- \equiv \frac{1 + \sqrt{1 - \frac{2M_\psi^2}{p_0v}}}{2}. \quad (125)$$

¹⁰we can understand this intuitively by the fact that the vertex $\propto v h \psi \bar{\psi}$ only exists on the higgsed, broken side.

A.2 Dimension six operator

Let us now consider the dimension 6 operator between scalars and gauge bosons of the form

$$\frac{h^2 F_{\mu\nu} F^{\mu\nu}}{\Lambda^2}, \quad (126)$$

where F is the field strength of a dark vector γ . In this section we study the splitting $h \rightarrow \gamma\gamma$, the kinematics are given as usual by

$$p_a = (p_0, 0, 0, p_0), \quad (127)$$

$$p_b = ((1-x)p_0, k_\perp, 0, \sqrt{(1-x)^2 p_0^2 - k_\perp^2 - M_\gamma^2}), \quad (128)$$

$$p_c = (xp_0, -k_\perp, 0, \sqrt{x^2 p_0^2 - k_\perp^2 - M_\gamma^2}), \quad (129)$$

We will work in the unitary gauge where the ghosts and the Goldstone boson have an infinite mass and are thus decoupled from the theory. We are thus left with only massive gauge bosons, two transverse modes \pm and one longitudinal mode 0. We first consider the two transverse polarization vectors, which are given by

$$\begin{aligned} \epsilon_b^\pm &= \frac{1}{\sqrt{2 - 2\frac{M_\gamma^2}{(1-x)^2 p_0^2}}} \left(0, \sqrt{1 - \frac{k_\perp^2 + M_\gamma^2}{(1-x)^2 p_0^2}}, \pm i \sqrt{1 - \frac{M_\gamma^2}{(1-x)^2 p_0^2}}, -\frac{k_\perp}{(1-x)p_0} \right), \\ \epsilon_c^\pm &= \frac{1}{\sqrt{2 - 2\frac{M_\gamma^2}{x^2 p_0^2}}} \left(0, \sqrt{1 - \frac{k_\perp^2 + M_\gamma^2}{x^2 p_0^2}}, \pm i \sqrt{1 - \frac{M_\gamma^2}{x^2 p_0^2}}, \frac{k_\perp}{xp_0} \right). \end{aligned} \quad (130)$$

Since in the frame transition $p_0 \gg M_\psi$, we can apply a massless limit and one obtains the following scalar products:

$$p_b \cdot \epsilon_b = 0, \quad (131)$$

$$\epsilon_b^- \cdot \epsilon_c^- \approx \epsilon_b^+ \cdot \epsilon_c^+ \approx \frac{k_\perp^2}{4p_0^2 x^2 (1-x)^2} \rightarrow 0, \quad (132)$$

$$\epsilon_b^- \cdot \epsilon_c^+ \approx \epsilon_b^+ \cdot \epsilon_c^- \approx -1 + \frac{k_\perp^2}{4p_0^2 x^2 (1-x)^2} \rightarrow -1, \quad (133)$$

$$p_b \cdot \epsilon_c^{+/-} \approx -\frac{k_\perp}{\sqrt{2}x} + \frac{k_\perp(k_\perp^2 x - M_\gamma^2(1-2x))}{2\sqrt{2}x^3(1-x)p_0^2} \rightarrow -\frac{k_\perp}{\sqrt{2}x}, \quad (134)$$

$$p_c \cdot \epsilon_b^{+/-} \approx \frac{k_\perp}{\sqrt{2}(1-x)} - \frac{k_\perp(k_\perp^2(1-x) + M_\gamma^2(1-2x))}{2\sqrt{2}x(1-x)^3 p_0^2} \rightarrow \frac{k_\perp}{\sqrt{2}(1-x)}, \quad (135)$$

$$p_b \cdot p_c \approx \frac{k_\perp^2 + M_\gamma^2(1-2x(1-x))}{2x(1-x)} + \frac{(k_\perp^2 + M_\gamma^2)^2(1-2x)^2}{8(1-x)^3 x^3 p_0^2} \rightarrow \frac{k_\perp^2 + M_\gamma^2(1-2x(1-x))}{2x(1-x)}, \quad (136)$$

which simplifies in the limit $p_0 \gg k_\perp > M_\psi$ by the quantity designated by the arrow. As before the vertex on the symmetric side is zero while the vertex on the higgsed side takes the form

$$V_h^{\lambda\lambda'} = \frac{2v}{\Lambda^2} ((p_b \cdot p_c)(\epsilon_b^\lambda \cdot \epsilon_c^{\lambda'}) - (p_c \cdot \epsilon_b^{\lambda'})(p_b \cdot \epsilon_c^\lambda)). \quad (137)$$

which gives after plugging Eq.(131)

$$V_h^{++} = V_h^{--} = \frac{v}{\Lambda^2} \frac{k_\perp^2}{x(1-x)}, \quad V_h^{+-} = V_h^{-+} = -\frac{v}{\Lambda^2} \frac{M_\gamma^2(1-2x(1-x))}{x(1-x)}. \quad (138)$$

Keeping only the leading order terms in k_\perp^2/p_0^2 , we obtain the following expression for the vertex function squared and summing over the polarisations, we obtain

$$|V_h|^2 \equiv |V_h^{++}|^2 + |V_h^{--}|^2 + 2|V_h^{+-}|^2 \approx \frac{v^2}{\Lambda^4} \frac{2}{x^2(1-x)^2} (k_\perp^4 + M_\gamma^4(1-2x(1-x))^2), \quad (139)$$

and consequently, using Eq.(117), we have

$$|\mathcal{M}_{h \rightarrow \gamma\gamma}|^2 \approx \frac{8(p_0 v)^2}{(M_\gamma^2 + k_\perp^2)^2 \Lambda^4} (k_\perp^4 + M_\gamma^4 (1 - 2(1-x)x)^2) \approx \frac{8(p_0 v)^2 k_\perp^4}{(M_\gamma^2 + k_\perp^2)^2 \Lambda^4}, \quad (140)$$

for negligible M_γ . As before, the probability of emission of transverse gauge bosons is obtained in the following way

$$P_{h \rightarrow \gamma\gamma}^T \approx \frac{1}{8p_0^2} \int_{b_+}^{b_-} \frac{dx}{x(1-x)} \int_0^{2p_0 v x(1-x) - M_\gamma^2} \frac{dk_\perp^2}{8\pi^2} |\mathcal{M}|^2 \quad (141)$$

$$\approx \frac{v^2 M_\gamma^2}{8\pi^2 \Lambda^4} \int_{b_+}^{b_-} \frac{dx}{x(1-x)} \int_0^{2p_0 v x(1-x)/M_\gamma^2} d\left(\frac{k_\perp^2}{M_\gamma^2}\right) \frac{(k_\perp^4/M_\gamma^4)}{(1 + (k_\perp/M_\gamma)^2)^2} \quad (142)$$

where we defined

$$b_+ \equiv \frac{1 - \sqrt{1 - \frac{2M_\gamma^2}{p_0 v}}}{2}, \quad b_- \equiv \frac{1 + \sqrt{1 - \frac{2M_\gamma^2}{p_0 v}}}{2}. \quad (143)$$

The function in the last integrand tends rapidly to one and we can therefore approximate it with unity so that the expression becomes

$$P_{h \rightarrow \gamma\gamma} \approx \frac{2p_0 v^3}{8\pi^2 \Lambda^4} \int_{b_+}^{b_-} dx \approx \frac{v^3 p_0}{4\pi^2 \Lambda^4} \sqrt{1 - \frac{2M_\gamma^2}{p_0 v}} \rightarrow \frac{v^3 p_0}{4\pi^2 \Lambda^4}, \quad (144)$$

Incidentally, the production of gluons from h via

$$\frac{h^2 G_{\mu\nu} G^{\mu\nu}}{\Lambda^2} \quad (145)$$

is of the same form

$$P_{h \rightarrow gg} = P_{h \rightarrow \gamma\gamma} \quad (146)$$

B Pressure on the bubble wall from particles production

In Ref. [59], it was pointed out that the production of heavy particles by the bubble wall is accompanied by an exchange of momentum from the plasma to the bubble: each produced pair of ψ particles act as a kick on the bubble wall, which appears as an effective pressure on the bubble wall when we integrate over the incoming flux. In this appendix, we recompute the pressure in the relativistic regime induced by particles produced via $h \rightarrow XX$.

Lorentz violating interactions will transfer momentum from the plasma to the wall. This *momentum* exchange can be identified with the loss of the momentum from the emitted particles, which in a $1 \rightarrow 2$ process, takes the form

$$\Delta p_z = p_a^z - p_b^z - p_c^z, \quad (147)$$

and can be evaluated from the kinematics in Eq.(116). The pressure on the wall can thus be identified with the convolution of this exchange of momentum and the probability of the interaction, together with the incoming flux,

$$\mathcal{P}_{a \rightarrow bc} = \underbrace{\int \frac{d^3 p}{(2\pi)^3} f_h(p_a)}_{\text{incoming flux}} \int dP_{a \rightarrow bc} \times \Delta p_z. \quad (148)$$

Using now the probability of the emission $h \rightarrow XX$,

$$dP_{a \rightarrow bc} = \frac{d^3 p_b d^3 p_c}{(2\pi)^6 2E_b 2E_c} |\mathcal{M}_{a \rightarrow bc}|^2 (2\pi)^3 \delta^2\left(\sum_i p_\perp^i\right) \delta\left(\sum_i E^i\right), \quad (149)$$

we will compute this integral for the different cases we have considered in the main text.

B.1 Dimension five operator

Let us first consider the computation of the pressure from the production of $X = \psi$ dark matter. In the regime of a fast bubble wall $(1-x)^2 x^2 p_0^2 \gg M_\psi^2 + k_\perp^2$,

$$\Delta p_z \approx \frac{M_\psi^2 + k_\perp^2}{2x(1-x)p_0}, \quad (150)$$

and the pressure can be computed with the following steps

$$\begin{aligned} \mathcal{P}_{h \rightarrow \psi\psi} &\approx 2 \frac{v^2}{\Lambda^2} \int \frac{d^3 p}{(2\pi)^3} f_h(p) \int_0^{2p_0 v x(1-x)} \frac{dk_\perp^2}{8\pi^2} \int_{k_\perp/p_0}^{1-k_\perp/p_0} \frac{dx}{(M_\psi^2 + k_\perp^2)} \times \frac{M_\psi^2 + k_\perp^2}{2x(1-x)p_0} \\ &= \frac{v^3}{\Lambda^2} \int \frac{d^3 p}{(2\pi)^3} f_h(p) \frac{1}{8\pi^2}, \end{aligned} \quad (151)$$

which finally leads to

$$\mathcal{P}_{h \rightarrow \psi\psi} \approx \frac{1}{8\pi^2} \frac{v^3 n_h \gamma_w}{\Lambda^2}. \quad (152)$$

B.2 Dimension six operator

We now turn to the pressure induced by the dimension six operator. We can easily estimate the pressure exerted on the bubble by multiplying with the production probability from Eq.(140) with exchange of momentum Δp_z and using the results in Eq.(148), we obtain

$$\begin{aligned} \mathcal{P}_{h \rightarrow \gamma\gamma} &\approx \int \frac{d^3 p}{(2\pi)^3} f_h(p) \frac{1}{4p_0^2} \int_0^{2vp_0 x(1-x)} \frac{dk_\perp^2}{8\pi^2} \int_{k_\perp/p_0}^{1-k_\perp/p_0} \frac{dx}{x(1-x)} \frac{k_\perp^2 + M_\gamma^2}{2x(1-x)p_0} \times \frac{8(p_0 v)^2 k_\perp^4}{(M_\gamma^2 + k_\perp^2)^2 \Lambda^4} \\ &\approx \int \frac{d^3 p}{(2\pi)^3} \frac{v^4}{\Lambda^4} \frac{p_0}{2\pi^2} f_h(p) \\ &\approx n_h \frac{v^4}{\Lambda^4} \frac{\gamma_w^2 T}{2\pi^2}. \end{aligned} \quad (153)$$

As for the particle production, the pressure is identical for vectors and for gluons

$$\mathcal{P}_{h \rightarrow gg} = \mathcal{P}_{h \rightarrow \gamma\gamma}. \quad (154)$$

C Computation of the Freeze-In abundance of DM

An irreducible contribution to the produced DM abundance comes from the high temperature Freeze-In via $2 \rightarrow 2$ scatterings. In this Appendix, we provide our estimates for the FI abundance via the different production channels that we considered in the main text.

C.1 Dimension five operator

If the h particles are in equilibrium with the thermal bath, the light DM particle will undergo Freeze-In via the $2 \rightarrow 2$ scatterings $hh \rightarrow \psi\bar{\psi}$. The scattering matrix is given by $|\mathcal{M}_{hh \rightarrow \psi\psi}|^2 = \frac{2}{\Lambda^2} (s - 4M_\psi^2)$ and the Boltzmann equation for this production mechanism takes the form [137]:

$$\begin{aligned} \dot{n}_\psi + 3Hn_\psi &= a^{-3} \frac{d(a^3 n_\psi)}{dt} = \frac{T}{512\pi^6} \int_{s_{\min}}^{\infty} d\Omega ds \frac{P_{hh} P_{\psi\psi}}{\sqrt{s}} |\mathcal{M}_{hh \rightarrow \psi\psi}|^2 K_1(\sqrt{s}/T) \\ &\approx \frac{T^5 M_\psi}{8\pi^5 \Lambda^2} \times \sqrt{\frac{\pi T}{M_\psi}} e^{-2M_\psi/T} \end{aligned} \quad (155)$$

where we defined $P_{ij} \equiv \frac{\sqrt{s-(m_i+m_j)^2} \sqrt{s-(m_i-m_j)^2}}{2\sqrt{s}}$, with $P_{hh} \approx \sqrt{s}/2$ and $P_{\psi\psi} \approx \sqrt{s-4M_\psi^2}/2$. To obtain an analytical answer we applied the following approximation $(s-4M^2)^{3/2} = (s-4M^2)(s-$

$4M^2)^{1/2} \approx (s-4M^2)4T$ and we have checked that this is in good agreement numerically. In the second line we took the limit of $M_\psi \gg T$, which we will follow from now on. We have also approximated the $zK_1(z) \rightarrow \sqrt{\pi z/2}e^{-z} \approx \sqrt{\pi M_\psi/T}e^{-z}$. The density normalized to the entropy density, $Y_\psi^{\text{FI}} = n_\psi^{\text{FI}}/s$ will hence become

$$\begin{aligned}
a^{-3} \frac{d(a^3 n_\psi)}{dt} &= -HT^4 \frac{d\left(\frac{n_\psi}{T^3}\right)}{dT} = -HT^4 g_\star \frac{2\pi^2}{45} \frac{dY}{dT} \approx \frac{T^5 M_\psi}{8\pi^5 \Lambda^2} \times \sqrt{\frac{\pi T}{M_\psi}} e^{-2M_\psi/T} \\
\Leftrightarrow \frac{dY}{dT} &\approx -\frac{45 M_{\text{pl}}}{16g_\star^{3/2} \pi^7 1.66 \Lambda^2} \times \sqrt{\frac{\pi M_\psi}{T}} e^{-2M_\psi/T} \\
\Leftrightarrow Y_\psi^{\text{FI}} &\approx \frac{45 M_{\text{pl}}}{16g_\star^{3/2} \pi^{13/2} 1.66 \Lambda^2} \times \frac{M_\psi}{2} \left(\frac{T_{\text{reh}}}{M_\psi}\right)^{3/2} e^{-2M_\psi/T_{\text{reh}}} \quad , \quad (156)
\end{aligned}$$

where the last line is a fit of our numerical analysis. This translates into a DM fraction today of

$$\begin{aligned}
\Omega_{\psi,\text{today}}^{\text{FI}} h^2 &= \frac{M_\psi Y_\psi^{\text{FI}} s_0}{\rho_c/h^2} \\
&= 2.35 \times 10^8 \left(\frac{M_\psi}{\text{GeV}}\right) \frac{45 M_{\text{pl}}}{16g_\star^{3/2} \pi^{13/2} 1.66 \Lambda^2} \times \frac{M_\psi}{2} \left(\frac{T_{\text{reh}}}{M_\psi}\right)^{3/2} e^{-2M_\psi/T_{\text{reh}}} \\
&= 5.84 \times 10^4 \left(\frac{M_\psi}{\text{GeV}}\right) \frac{M_{\text{pl}} M_\psi}{g_\star^{3/2} \Lambda^2} \left(\frac{T_{\text{reh}}}{M_\psi}\right)^{3/2} e^{-2M_\psi/T_{\text{reh}}} \quad . \quad (157)
\end{aligned}$$

C.2 Dimension six operator: vectors

Let us repeat the same computation for the FI of massive vectors, the computation will follow the same steps. The scattering matrix for the vector portal is now given by

$$|\mathcal{M}_{hh \rightarrow \gamma\gamma}|^2 \approx \frac{1}{\Lambda^4} (2(s - 2M_\gamma^2)^2 + 4M_\gamma^4) \quad . \quad (158)$$

We will perform the computation in the two following limits: $M_\gamma \gg T$ and $M_\gamma \ll T$.

In the case, $M_\gamma \gg T$: The matrix element takes the form

$$|\mathcal{M}_{hh \rightarrow \gamma\gamma}|^2 \approx \frac{1}{\Lambda^4} (2(s - 2M_\gamma^2)^2 + 4M_\gamma^4) \approx \frac{12M_\gamma^4}{\Lambda^4} \quad (159)$$

where the second approximation comes from the fact that we consider the regime $M_\gamma \gg T$ where the exponential suppression selects the smallest value of the $s \approx 4M_\gamma^2$. The Boltzmann equations for this production take the form

$$\begin{aligned}
\dot{n}_\gamma + 3Hn_\gamma &= a^{-3} \frac{d(a^3 n_\gamma)}{dt} = \frac{T}{512\pi^6} \int_{s_{\text{min}}}^{\infty} d\Omega ds \frac{P_{hh} P_{\gamma\gamma}}{\sqrt{s}} |\mathcal{M}_{hh \rightarrow \gamma\gamma}|^2 K_1(\sqrt{s}/T) \\
&\approx \frac{3T^4 M_\gamma^4}{32\pi^9/2 \Lambda^4} \times \sqrt{\frac{M_\gamma}{T}} e^{-2M_\gamma/T} \quad , \quad (160)
\end{aligned}$$

where we again applied $(s - 4M_\gamma^2)^{1/2} \approx 2T$. It follows that

$$\begin{aligned}
\frac{dY_\gamma^{\text{FI}}}{dT} &\approx \frac{135 M_{\text{pl}} M_\gamma^4}{64\pi^{13/2} g_\star^{3/2} 1.66 T^2 \Lambda^4} \sqrt{\frac{M_\gamma}{T}} e^{-2M_\gamma/T} \\
Y_\gamma^{\text{FI}} &\approx \frac{135 M_{\text{pl}} M_\gamma^3}{128\pi^{13/2} g_\star^{3/2} 1.66 \Lambda^4} \sqrt{\frac{M_\gamma}{T_{\text{reh}}}} e^{-2M_\gamma/T_{\text{reh}}} \quad . \quad (161)
\end{aligned}$$

Finally

$$\begin{aligned}
\Omega_{\gamma, \text{today}}^{\text{FI}} h^2 &= \frac{M_\gamma Y_\gamma^{\text{FI}} s_0}{\rho_c / h^2} \\
&\approx 2.35 \times 10^8 \left(\frac{M_\gamma}{\text{GeV}} \right) \frac{135 M_{\text{pl}} M_\gamma^3}{128 \pi^{13/2} g_\star^{3/2} 1.66 \Lambda^4} \sqrt{\frac{M_\gamma}{T_{\text{reh}}}} e^{-2M_\gamma/T_{\text{reh}}} \\
&\approx 8.76 \times 10^4 \left(\frac{M_\gamma}{\text{GeV}} \right) \frac{M_{\text{pl}} M_\gamma^3}{g_\star^{3/2} \Lambda^4} \sqrt{\frac{M_\gamma}{T_{\text{reh}}}} e^{-2M_\gamma/T_{\text{reh}}}.
\end{aligned} \tag{162}$$

In the case, $M_\gamma \ll T$: In the case of relativistic FI, we obtain

$$|\mathcal{M}|_{hh \rightarrow \gamma\gamma}^2 \simeq \frac{2s^2}{\Lambda^4} \quad a^{-3} \frac{d(a^3 n_\gamma)}{dt} \approx \frac{3T^8}{\pi^5 \Lambda^4}, \tag{163}$$

which leads to

$$Y_{\text{FI}}^{M_\gamma \ll T} \approx \frac{45 M_{\text{pl}} T_{\text{reh}}^3}{3.32 \pi^7 g_\star^{3/2} \Lambda^4}, \tag{164}$$

and Finally

$$\begin{aligned}
Y_{\text{FI}}^{M_\gamma \ll T} h^2 &= \frac{M_\gamma Y_\gamma^{\text{FI}} s_0}{\rho_c / h^2} \\
&\approx 2.35 \times 10^8 \left(\frac{M_\gamma}{\text{GeV}} \right) \frac{45 M_{\text{pl}} T_{\text{reh}}^3}{3.32 \pi^7 g_\star^{3/2} \Lambda^4} \\
&\approx 1.05 \times 10^6 \left(\frac{M_\gamma}{\text{GeV}} \right) \frac{M_{\text{pl}} T_{\text{reh}}^3}{g_\star^{3/2} \Lambda^4}.
\end{aligned} \tag{165}$$

C.3 Dimension six operator: gluons

We now compute the Freeze-In density for gluons, keeping in mind the requirement $M_G \lesssim v$, and so $M_G \lesssim T_R$. In this section T_{reh} is the reheating temperature. There should be several regimes of FI. Typical gluons, during FI, will be produced with energy $E_g \sim T_R \gtrsim M_G$. We will focus however only on the case in which the dark sector reaches a gluon plasma.

If the following condition is fulfilled

$$\rho_g^{\text{FI}} \gg \Lambda_{\text{conf}}^4, \tag{166}$$

the dark sector will immediately go back to a plasma of free thermal gluons, then the

$$\begin{aligned}
\dot{\rho}_g + 4H\rho_g &= \frac{3T}{512\pi^6} \int_0^\infty d\Omega ds \frac{s}{4} |\mathcal{M}|_{\phi\phi \rightarrow gg}^2 K_1(\sqrt{s}/T) \\
&= \frac{3(N^2 - 1)T}{256\pi^5 \Lambda^4} \int_0^\infty ds s^3 K_1(\sqrt{s}/T) \\
&= \frac{4725(N^2 - 1)T^9}{256\pi^5 \Lambda^4}.
\end{aligned} \tag{167}$$

The density normalized to the entropy density, $Y_\psi^{\text{FI}} = \frac{n_\psi^{\text{FI}}}{s}$ will hence become

$$\begin{aligned}
\dot{\rho}_g + 4H\rho_g &= -HT^5 \frac{d(T^{-4} \rho_g)}{dT} = \frac{4725(N^2 - 1)T^9}{256\pi^5 \Lambda^4} \\
\Leftrightarrow \frac{\rho_g}{T^4} \Big|_{\text{FI}} &= \int_0^{T_{\text{reh}}} dT \frac{4725(N^2 - 1)T^2 M_{\text{Pl}}}{256\sqrt{g_\star} 1.66\pi^5 \Lambda^4} = 10.2 \frac{(N^2 - 1)T_{\text{reh}}^3 M_{\text{Pl}}}{\sqrt{g_\star} \pi^5 \Lambda^4}
\end{aligned} \tag{168}$$

which correspond to a temperature of the dark sector being

$$\left(\frac{T_g}{T_\gamma} \right)^4 \approx 150 \frac{T_{\text{reh}}^3 M_{\text{Pl}}}{\sqrt{g_\star} \pi^7 \Lambda^4}. \tag{169}$$

D Computation of the instantaneous spectrum after production

In this appendix, we present the computations of the spectrum of boosted particles immediately after emission. We will first present a few analytical results and then provide the numerical method we followed for the full computation of the spectrum that appears in the main text.

D.1 Energy distributions

Let us calculate the energy distribution for the particles in the plasma-bubble wall collisions. We will now compute the energy spectrum immediately after the DM production from bubble expansion.

D.1.1 Dimension 5 operator computation

We will start the discussion with the case of the dimension five operator. The average value of the transverse momenta of the field ψ will be given by, for an incoming h particle with fixed momentum p ,

$$\bar{k}_\perp \equiv \frac{\int d^3p P_{h \rightarrow \psi\psi} f_h(p) k_\perp}{\int d^3p P_{h \rightarrow \psi\psi} f_h(p)}, \quad \bar{k}_\perp^2 \equiv \frac{\int d^3p P_{h \rightarrow \psi\psi} f_h(p) k_\perp^2}{\int d^3p P_{h \rightarrow \psi\psi} f_h(p)}, \quad (170)$$

which reduce to

$$\begin{aligned} \bar{k}_\perp &= \frac{\int \frac{dk_\perp^2 dx}{(k_\perp^2 + M_\psi^2)^2} \left[k_\perp^2 + M_\psi^2 (2x - 1)^2 \right] k_\perp}{\int \frac{dk_\perp^2 dx}{(k_\perp^2 + M_\psi^2)^2} \left[k_\perp^2 + M_\psi^2 (2x - 1)^2 \right]} \quad \text{with} \quad \frac{k_\perp^2 + M_\psi^2}{2p_0 x (1 - x)} < L_w^{-1} \\ \Rightarrow \quad \bar{k}_\perp &= \frac{\pi \sqrt{p_0 L_w^{-1}}}{2\sqrt{2} (\log \frac{p_0 L_w^{-1}}{M_\psi^2} - 8/3 + \log 2)}, \quad \bar{k}_\perp^2 \simeq \frac{L_w^{-1} p_0}{3 \log \left(\frac{p_0 L_w^{-1}}{M_\psi^2} \right) - 5.92}. \end{aligned} \quad (171)$$

Armed with this expression we can estimate the average energy of the ψ field in the plasma frame $\bar{E}_{\psi \text{ plasma}}$, assuming that the incoming particle h , which produces ψ , has energy $p_0 \sim p_z$. We obtain

$$\bar{E}_{\psi \text{ plasma}} = \gamma_w (E_\psi - v_w \sqrt{E_\psi^2 - k_\perp^2 - M_\psi^2}) \approx \gamma_w \frac{\bar{k}_\perp^2}{2E_\psi}, \quad (172)$$

where E_ψ is the energy of the ψ field in the wall frame and scales like $\sim T\gamma_w$. In this case, we can expand for very large values of γ_w and use the expression for the average value of \bar{k}_\perp^2 to find

$$\bar{E}_{\psi} \simeq \frac{L_w^{-1} \gamma_w}{3 \log \frac{\gamma_w T}{M_\psi^2 L_w} - 5.92}, \quad (173)$$

where we took $2E_\psi \approx p_0$, corresponding to $x \approx 1/2$. This analytical computation does not take into account the necessary convolution with the Boltzmann distribution of the incoming h .

D.1.2 Dimension 6 operator computation

For the dimension six case, the computation proceeds in a similar way. We can again neglect the mass of the M_γ in the computation and the expressions simplify to

$$\bar{k}_\perp^2 \simeq \frac{p_0 (17 - 24 \log(2))}{6L_w (\log(4) - 1)} \approx 0.16 p_0 L_w^{-1}. \quad (174)$$

$$\bar{k}_\perp \simeq -\frac{(16\sqrt{2} - 23) \pi p_0}{6\sqrt{2} (\log(4) - 1) \sqrt{L_w p_0}} \approx 0.36 \sqrt{p_0 L_w^{-1}} \quad (175)$$

The average energy in the plasma frame will then become

$$\bar{E}_{\gamma \text{ plasma}}^{\text{analytical}} \approx \gamma_w \frac{\bar{k}_\perp^2}{2E_\gamma} \approx 0.16 \gamma_w L_w^{-1}, \quad (176)$$

where we again took $2E_\gamma \approx p_0$ since $x \approx \frac{1}{2}$.

D.2 Numerical algorithm for the evaluation of the spectrum

We have also calculated numerically the distribution function with respect to the energy of the ψ field. This can be done by convoluting the distribution of the initial particle with the corresponding δ function

$$\frac{dF}{dE} = \frac{\int d^3p f_h(p) \int dk_{\perp}^2 dx |\mathcal{M}_{h \rightarrow XX}|^2 \delta(E - E(p_0^h, p_z, x, k_{\perp}))}{\text{Normalization}}$$

$$E(E, p_z, x, k_{\perp}) = p_0^h x \gamma_w - \sqrt{\gamma_w^2 - 1} \sqrt{(p_0^h x)^2 - M^2 - k_{\perp}^2}, \quad (177)$$

where the integral is performed using the Monte-Carlo method and E (M) is the energy (mass) of the emitted particle, being E_{ψ}, E_{γ} (M_{ψ}, M_{γ}). The overall normalization factor is determined at the end requiring

$$\int \frac{dF}{dE} dE = 1. \quad (178)$$

The numerical procedure becomes more efficient if we introduce a new integration variable:

$$Y = \frac{\gamma_w}{T} (p_0^h - v p_z^h) \Rightarrow d^3p f_h(p) \propto dY dp_z e^{-Y} \left(\frac{TY}{\gamma_w} + v_w p_h \right). \quad (179)$$

Note that we have ignored the overall numerical factor in front since the normalization is anyway determined at the end by Eq.(183). The results of this procedure for the spectrum are shown in Fig.2 and Fig.4, for the fermion and the vector production respectively, and we see that the distribution is peaked around the average energy value \bar{E} and drops exponentially fast once the threshold $L_w^{-1} \gamma_w$ is passed. One can see the origin of this threshold from the following (expanding Eq.172):

$$\bar{E}_{\text{plasma}} \simeq \frac{E}{2\gamma_w} + \frac{k_{\perp}^2 \gamma_w}{2E} \approx \frac{k_{\perp}^2 \gamma_w}{p_0^h}, \quad (180)$$

where we took $p_0 \approx 2E$. On the other hand the maximum value of k_{\perp}^2 is

$$k_{\perp}^2|_{\text{MAX}} \sim p_0^h L_w^{-1}, \quad (181)$$

from non-adiabaticity arguments, thus we obtain

$$\bar{E}_{\text{plasma}}|_{\text{MAX}} \simeq L_w^{-1} \gamma_w, \quad (182)$$

so we expect the sharp drop of the spectrum once the threshold is passed. Using the spectrum, computed via this method, also allows us to compute the average energy in the plasma frame by simple integration of it.

D.2.1 Numerical determination of the average energies

After having computed the spectrum numerically, we can also extract the average energy via

$$\bar{E} = \int \frac{dF}{dE} E dE. \quad (183)$$

and we obtain a good fit of the numerical data with

$$\bar{E}_{\psi \text{ plasma}}^{\text{numerical}} \simeq (0.5 - 1) \frac{L_w^{-1} \gamma_w}{3 \log \frac{\gamma_w T}{M_{\psi}^2 L_w} - 5.92}, \quad (184)$$

for the dimension five production and

$$\bar{E}_{\gamma \text{ plasma}}^{\text{numerical}} \approx (0.12 - 0.17) \gamma_w L_w^{-1}, \quad (185)$$

for the dimension six production. This agrees well with the analytical computations.

References

- [1] V. A. Kuzmin, V. A. Rubakov, and M. E. Shaposhnikov *Phys. Lett. B* **155** (1985) 36.
- [2] M. Shaposhnikov *JETP Lett.* **44** (1986) 465–468.
- [3] A. E. Nelson, D. B. Kaplan, and A. G. Cohen *Nucl. Phys. B* **373** (1992) 453–478.
- [4] M. Carena, M. Quiros, and C. E. M. Wagner *Phys. Lett. B* **380** (1996) 81–91, [[hep-ph/9603420](#)].
- [5] J. M. Cline *Phil. Trans. Roy. Soc. Lond. A* **376** (2018), no. 2114 20170116, [[arXiv:1704.08911](#)].
- [6] A. J. Long, A. Tesi, and L.-T. Wang *JHEP* **10** (2017) 095, [[arXiv:1703.04902](#)].
- [7] S. Bruggisser, B. Von Harling, O. Matsedonskyi, and G. Servant *JHEP* **12** (2018) 099, [[arXiv:1804.07314](#)].
- [8] S. Bruggisser, B. Von Harling, O. Matsedonskyi, and G. Servant *Phys. Rev. Lett.* **121** (2018), no. 13 131801, [[arXiv:1803.08546](#)].
- [9] D. E. Morrissey and M. J. Ramsey-Musolf *New J. Phys.* **14** (2012) 125003, [[arXiv:1206.2942](#)].
- [10] A. Azatov, M. Vanvlasselaer, and W. Yin *JHEP* **10** (2021) 043, [[arXiv:2106.14913](#)].
- [11] P. Huang and K.-P. Xie *JHEP* **09** (2022) 052, [[arXiv:2206.04691](#)].
- [12] I. Baldes, S. Blasi, A. Mariotti, A. Sevrin, and K. Turbang [arXiv:2106.15602](#).
- [13] I. Baldes, S. Blasi, A. Mariotti, A. Sevrin, and K. Turbang [arXiv:2106.15602](#).
- [14] E. J. Chun, T. P. Dutka, T. H. Jung, X. Nagels, and M. Vanvlasselaer [arXiv:2305.10759](#).
- [15] A. Falkowski and J. M. No *JHEP* **02** (2013) 034, [[arXiv:1211.5615](#)].
- [16] I. Baldes, Y. Gouttenoire, and F. Sala *JHEP* **04** (2021) 278, [[arXiv:2007.08440](#)].
- [17] J.-P. Hong, S. Jung, and K.-P. Xie *Phys. Rev. D* **102** (2020), no. 7 075028, [[arXiv:2008.04430](#)].
- [18] A. Azatov, M. Vanvlasselaer, and W. Yin *JHEP* **03** (2021) 288, [[arXiv:2101.05721](#)].
- [19] I. Baldes, Y. Gouttenoire, F. Sala, and G. Servant *JHEP* **07** (2022) 084, [[arXiv:2110.13926](#)].
- [20] P. Asadi, E. D. Kramer, E. Kuflik, G. W. Ridgway, T. R. Slatyer, and J. Smirnov *Phys. Rev. D* **104** (2021), no. 9 095013, [[arXiv:2103.09827](#)].
- [21] P. Lu, K. Kawana, and K.-P. Xie *Phys. Rev. D* **105** (2022), no. 12 123503, [[arXiv:2202.03439](#)].
- [22] I. Baldes, Y. Gouttenoire, and F. Sala *SciPost Phys.* **14** (2023) 033, [[arXiv:2207.05096](#)].
- [23] A. Azatov, G. Barni, S. Chakraborty, M. Vanvlasselaer, and W. Yin *JHEP* **10** (2022) 017, [[arXiv:2207.02230](#)].
- [24] I. Baldes, M. Dichtl, Y. Gouttenoire, and F. Sala [arXiv:2306.15555](#).
- [25] M. Kierkla, A. Karam, and B. Swiezewska *JHEP* **03** (2023) 007, [[arXiv:2210.07075](#)].
- [26] G. F. Giudice, H. M. Lee, A. Pomarol, and B. Shakya [arXiv:2403.03252](#).
- [27] H. Kodama, M. Sasaki, and K. Sato *Progress of Theoretical Physics* **68** (12, 1982) 1979–1998, [<https://academic.oup.com/ptp/article-pdf/68/6/1979/5311817/68-6-1979.pdf>].
- [28] K. Kawana and K.-P. Xie *Phys. Lett. B* **824** (2022) 136791, [[arXiv:2106.00111](#)].
- [29] T. H. Jung and T. Okui [arXiv:2110.04271](#).
- [30] Y. Gouttenoire and T. Volansky [arXiv:2305.04942](#).
- [31] M. Lewicki, P. Toczek, and V. Vaskonen [arXiv:2305.04924](#).
- [32] E. Witten *Phys. Rev.* **D30** (1984) 272–285.
- [33] C. J. Hogan *Mon. Not. Roy. Astron. Soc.* **218** (1986) 629–636.
- [34] A. Kosowsky and M. S. Turner *Phys. Rev.* **D47** (1993) 4372–4391, [[astro-ph/9211004](#)].
- [35] A. Kosowsky, M. S. Turner, and R. Watkins *Phys. Rev. Lett.* **69** (1992) 2026–2029.
- [36] M. Kamionkowski, A. Kosowsky, and M. S. Turner *Phys. Rev.* **D49** (1994) 2837–2851, [[astro-ph/9310044](#)].
- [37] J. R. Espinosa, T. Konstandin, J. M. No, and G. Servant *JCAP* **1006** (2010) 028, [[arXiv:1004.4187](#)].
- [38] R. Pasechnik, M. Reichert, F. Sannino, and Z.-W. Wang *JHEP* **02** (2024) 159, [[arXiv:2309.16755](#)].
- [39] A. Azatov and M. Vanvlasselaer *JHEP* **09** (2020) 085, [[arXiv:2003.10265](#)].
- [40] M. T. Frandsen, M. Heikinheimo, M. Rosenlyst, M. E. Thing, and K. Tuominen *JHEP* **09** (2023) 022, [[arXiv:2302.09104](#)].
- [41] M. Reichert and Z.-W. Wang *EPJ Web Conf.* **274** (2022) 08003, [[arXiv:2211.08877](#)].
- [42] K. Fujikura, Y. Nakai, R. Sato, and Y. Wang *JHEP* **09** (2023) 053, [[arXiv:2306.01305](#)].
- [43] C. Delaunay, C. Grojean, and J. D. Wells *JHEP* **04** (2008) 029, [[arXiv:0711.2511](#)].
- [44] G. Kurup and M. Perelstein *Phys. Rev. D* **96** (2017), no. 1 015036, [[arXiv:1704.03381](#)].
- [45] B. von Harling and G. Servant *JHEP* **01** (2018) 159, [[arXiv:1711.11554](#)].

- [46] A. Azatov, D. Barducci, and F. Sgarlata *JCAP* **07** (2020) 027, [[arXiv:1910.01124](#)].
- [47] T. Ghosh, H.-K. Guo, T. Han, and H. Liu *JHEP* **07** (2021) 045, [[arXiv:2012.09758](#)].
- [48] M. Aoki, T. Komatsu, and H. Shibuya *PTEP* **2022** (2022), no. 6 063B05, [[arXiv:2106.03439](#)].
- [49] M. Badziak and I. Nalecz *JHEP* **02** (2023) 185, [[arXiv:2212.09776](#)].
- [50] S. Blasi and A. Mariotti [arXiv:2203.16450](#).
- [51] U. Banerjee, S. Chakraborty, S. Prakash, and S. U. Rahaman [arXiv:2402.02914](#).
- [52] L. Delle Rose, G. Panico, M. Redi, and A. Tesi *JHEP* **04** (2020) 025, [[arXiv:1912.06139](#)].
- [53] B. Von Harling, A. Pomarol, O. Pujolàs, and F. Rompineve *JHEP* **04** (2020) 195, [[arXiv:1912.07587](#)].
- [54] J. Halverson, C. Long, A. Maiti, B. Nelson, and G. Salinas *JHEP* **05** (2021) 154, [[arXiv:2012.04071](#)].
- [55] E. Morgante, N. Ramberg, and P. Schwaller *Phys. Rev. D* **107** (2023), no. 3 036010, [[arXiv:2210.11821](#)].
- [56] R. Jinno and M. Takimoto *Phys. Rev. D* **95** (2017), no. 1 015020, [[arXiv:1604.05035](#)].
- [57] A. Addazi, A. Marcianò, A. P. Morais, R. Pasechnik, J. a. Viana, and H. Yang *JCAP* **09** (2023) 026, [[arXiv:2304.02399](#)]. [Erratum: *JCAP* 03, E01 (2024)].
- [58] D. Bodeker and G. D. Moore *JCAP* **1705** (2017), no. 05 025, [[arXiv:1703.08215](#)].
- [59] A. Azatov and M. Vanvlasselaer *JCAP* **01** (2021) 058, [[arXiv:2010.02590](#)].
- [60] I. Baldes, M. Dichtl, Y. Gouttenoire, and F. Sala [arXiv:2403.05615](#).
- [61] P. Minkowski *Phys. Lett. B* **67** (1977) 421–428.
- [62] T. Yanagida *Conf. Proc. C* **7902131** (1979) 95–99.
- [63] P. Ramond, *The Family Group in Grand Unified Theories*, in *International Symposium on Fundamentals of Quantum Theory and Quantum Field Theory*, 2, 1979. [hep-ph/9809459](#).
- [64] M. Gell-Mann, P. Ramond, and R. Slansky *Conf. Proc. C* **790927** (1979) 315–321, [[arXiv:1306.4669](#)].
- [65] R. N. Mohapatra and G. Senjanovic *Phys. Rev. Lett.* **44** (1980) 912.
- [66] J. E. Kim *Phys. Rev. Lett.* **43** (1979) 103.
- [67] M. A. Shifman, A. I. Vainshtein, and V. I. Zakharov *Nucl. Phys. B* **166** (1980) 493–506.
- [68] M. Dine, W. Fischler, and M. Srednicki *Phys. Lett. B* **104** (1981) 199–202.
- [69] A. R. Zhitnitsky *Sov. J. Nucl. Phys.* **31** (1980) 260.
- [70] K. Yamamoto *Phys. Lett. B* **168** (1986) 341–346.
- [71] D. H. Lyth and E. D. Stewart *Phys. Rev. D* **53** (1996) 1784–1798, [[hep-ph/9510204](#)].
- [72] A. Azatov, G. Barni, and R. Petrossian-Byrne [arXiv:2405.19447](#).
- [73] P. Bode, J. P. Ostriker, and N. Turok *Astrophys. J.* **556** (2001) 93–107, [[astro-ph/0010389](#)].
- [74] M. Viel, J. Lesgourgues, M. G. Haehnelt, S. Matarrese, and A. Riotto *Phys. Rev. D* **71** (2005) 063534, [[astro-ph/0501562](#)].
- [75] V. Iršič et al. *Phys. Rev. D* **96** (2017), no. 2 023522, [[arXiv:1702.01764](#)].
- [76] M. Sitwell, A. Mesinger, Y.-Z. Ma, and K. Sigurdson *Mon. Not. Roy. Astron. Soc.* **438** (2014), no. 3 2664–2671, [[arXiv:1310.0029](#)].
- [77] J. B. Muñoz, C. Dvorkin, and F.-Y. Cyr-Racine *Phys. Rev. D* **101** (2020), no. 6 063526, [[arXiv:1911.11144](#)].
- [78] **LSST Dark Matter Group** Collaboration, A. Drlica-Wagner et al. [arXiv:1902.01055](#).
- [79] S. Colombi, S. Dodelson, and L. M. Widrow *Astrophys. J.* **458** (1996) 1, [[astro-ph/9505029](#)].
- [80] H. Mansour and B. Shakya [arXiv:2308.13070](#).
- [81] B. Shakya [arXiv:2308.16224](#).
- [82] K. Enqvist, J. Ignatius, K. Kajantie, and K. Rummukainen *Phys. Rev. D* **45** (May, 1992) 3415–3428.
- [83] J. Ellis, M. Lewicki, J. M. No, and V. Vaskonen *JCAP* **1906** (2019), no. 06 024, [[arXiv:1903.09642](#)].
- [84] M. Dine, R. G. Leigh, P. Y. Huet, A. D. Linde, and D. A. Linde *Phys. Rev.* **D46** (1992) 550–571, [[hep-ph/9203203](#)].
- [85] B.-H. Liu, L. D. McLerran, and N. Turok *Phys. Rev. D* **46** (1992) 2668–2688.
- [86] G. D. Moore and T. Prokopec *Phys. Rev. Lett.* **75** (1995) 777–780, [[hep-ph/9503296](#)].
- [87] G. D. Moore and T. Prokopec *Phys. Rev.* **D52** (1995) 7182–7204, [[hep-ph/9506475](#)].
- [88] G. C. Dorsch, S. J. Huber, and T. Konstandin *JCAP* **1812** (2018), no. 12 034, [[arXiv:1809.04907](#)].
- [89] B. Laurent and J. M. Cline *Phys. Rev. D* **106** (2022), no. 2 023501, [[arXiv:2204.13120](#)].
- [90] S. Jiang, F. P. Huang, and X. Wang *Phys. Rev. D* **107** (2023), no. 9 095005, [[arXiv:2211.13142](#)].
- [91] T. Konstandin and J. M. No *JCAP* **02** (2011) 008, [[arXiv:1011.3735](#)].

- [92] M. Barroso Mancha, T. Prokopec, and B. Swiezevska *JHEP* **01** (2021) 070, [[arXiv:2005.10875](#)].
- [93] S. Balaaji, M. Spannowsky, and C. Tamarit *JCAP* **03** (2021) 051, [[arXiv:2010.08013](#)].
- [94] S.-J. Wang and Z.-Y. Yuwen *Phys. Rev. D* **107** (2023), no. 2 023501, [[arXiv:2205.02492](#)].
- [95] T. Krajewski, M. Lewicki, and M. Zych *Phys. Rev. D* **108** (2023), no. 10 103523, [[arXiv:2303.18216](#)].
- [96] M. Sanchez-Garitaonandia and J. van de Vis [arXiv:2312.09964](#).
- [97] D. Bodeker and G. D. Moore *JCAP* **0905** (2009) 009, [[arXiv:0903.4099](#)].
- [98] Y. Gouttenoire, R. Jinno, and F. Sala *JHEP* **05** (2022) 004, [[arXiv:2112.07686](#)].
- [99] W.-Y. Ai *JCAP* **10** (2023) 052, [[arXiv:2308.10679](#)].
- [100] A. Azatov, G. Barni, R. Petrossian-Byrne, and M. Vanvlasselaer [arXiv:2310.06972](#).
- [101] W.-Y. Ai, B. Garbrecht, and C. Tamarit *JCAP* **03** (2022), no. 03 015, [[arXiv:2109.13710](#)].
- [102] W.-Y. Ai, B. Laurent, and J. van de Vis *JCAP* **07** (2023) 002, [[arXiv:2303.10171](#)].
- [103] W.-Y. Ai, X. Nagels, and M. Vanvlasselaer *JCAP* **03** (2024) 037, [[arXiv:2401.05911](#)].
- [104] G. Barni, S. Blasi, and M. Vanvlasselaer [arXiv:2406.01596](#).
- [105] E. D. Carlson, M. E. Machacek, and L. J. Hall *Astrophys. J.* **398** (1992) 43–52.
- [106] Y. Hochberg, E. Kuflik, T. Volansky, and J. G. Wacker *Phys. Rev. Lett.* **113** (2014) 171301, [[arXiv:1402.5143](#)].
- [107] L. Forestell, D. E. Morrissey, and K. Sigurdson *Phys. Rev. D* **95** (2017), no. 1 015032, [[arXiv:1605.08048](#)].
- [108] M. Vogelsberger, J. Zavala, and A. Loeb *Mon. Not. Roy. Astron. Soc.* **423** (2012) 3740, [[arXiv:1201.5892](#)].
- [109] M. Vogelsberger, J. Zavala, C. Simpson, and A. Jenkins *Mon. Not. Roy. Astron. Soc.* **444** (2014), no. 4 3684–3698, [[arXiv:1405.5216](#)].
- [110] A. Zentner, S. Dandavate, O. Slone, and M. Lisanti *JCAP* **07** (2022), no. 07 031, [[arXiv:2202.00012](#)].
- [111] J. Pollack, D. N. Spergel, and P. J. Steinhardt *Astrophys. J.* **804** (2015), no. 2 131, [[arXiv:1501.00017](#)].
- [112] M. Redi, A. Tesi, and H. Tillim *JHEP* **05** (2021) 010, [[arXiv:2011.10565](#)].
- [113] D. Curtin, C. Gemme, and C. B. Verhaaren *Phys. Rev. D* **106** (2022), no. 7 075015, [[arXiv:2202.12899](#)].
- [114] R. K. Ellis, W. J. Stirling, and B. R. Webber, *QCD and collider physics*, vol. 8. Cambridge University Press, 2, 2011.
- [115] **TOTEM** Collaboration, G. Antchev et al. *Eur. Phys. J. C* **79** (2019), no. 2 103, [[arXiv:1712.06153](#)].
- [116] A. Kurkela and G. D. Moore *JHEP* **12** (2011) 044, [[arXiv:1107.5050](#)].
- [117] B. S. Acharya, M. Fairbairn, and E. Hardy *JHEP* **07** (2017) 100, [[arXiv:1704.01804](#)].
- [118] S. W. Randall, M. Markevitch, D. Clowe, A. H. Gonzalez, and M. Bradac *Astrophys. J.* **679** (2008) 1173–1180, [[arXiv:0704.0261](#)].
- [119] S. Tulin and H.-B. Yu *Phys. Rept.* **730** (2018) 1–57, [[arXiv:1705.02358](#)].
- [120] D. Song, K. Murase, and A. Kheirandish *JCAP* **03** (2024) 024, [[arXiv:2308.00589](#)].
- [121] T. Konstandin *JCAP* **1803** (2018), no. 03 047, [[arXiv:1712.06869](#)].
- [122] C. Caprini, D. G. Figueroa, R. Flauger, G. Nardini, M. Peloso, M. Pieroni, A. Ricciardone, and G. Tasinato *JCAP* **11** (2019) 017, [[arXiv:1906.09244](#)].
- [123] R. Flauger, N. Karnesis, G. Nardini, M. Pieroni, A. Ricciardone, and J. Torrado *JCAP* **01** (2021) 059, [[arXiv:2009.11845](#)].
- [124] G. Boileau, N. Christensen, R. Meyer, and N. J. Cornish *Phys. Rev. D* **103** (2021), no. 10 103529, [[arXiv:2011.05055](#)].
- [125] K. Martinovic, P. M. Meyers, M. Sakellariadou, and N. Christensen *Phys. Rev. D* **103** (2021), no. 4 043023, [[arXiv:2011.05697](#)].
- [126] C. J. Moore, R. H. Cole, and C. P. L. Berry *Class. Quant. Grav.* **32** (2015), no. 1 015014, [[arXiv:1408.0740](#)].
- [127] **KAGRA, LIGO Scientific, VIRGO** Collaboration, B. P. Abbott et al. *Living Rev. Rel.* **21** (2018), no. 1 3, [[arXiv:1304.0670](#)].
- [128] **LIGO Scientific** Collaboration, J. Aasi et al. *Class. Quant. Grav.* **32** (2015) 074001, [[arXiv:1411.4547](#)].
- [129] T. Robson, N. J. Cornish, and C. Liug *Class. Quant. Grav.* **36** (2019), no. 10 105011, [[arXiv:1803.01944](#)].
- [130] **MAGIS** Collaboration, P. W. Graham, J. M. Hogan, M. A. Kasevich, S. Rajendran, and R. W. Romani [arXiv:1711.02225](#).
- [131] K. Yagi, N. Tanahashi, and T. Tanaka *Phys. Rev.* **D83** (2011) 084036, [[arXiv:1101.4997](#)].
- [132] K. Yagi *Int. J. Mod. Phys.* **D22** (2013) 1341013, [[arXiv:1302.2388](#)].
- [133] B. Sathyaprakash et al. *Class. Quant. Grav.* **29** (2012) 124013, [[arXiv:1206.0331](#)]. [Erratum: *Class. Quant. Grav.*30,079501(2013)].

- [134] **KAGRA, Virgo, LIGO Scientific** Collaboration, R. Abbott et al. *Phys. Rev. D* **104** (2021), no. 2 022004, [[arXiv:2101.12130](#)].
- [135] G. Boileau, A. C. Jenkins, M. Sakellariadou, R. Meyer, and N. Christensen *Phys. Rev. D* **105** (2022), no. 2 023510, [[arXiv:2109.06552](#)].
- [136] G. Boileau, N. Christensen, C. Gowling, M. Hindmarsh, and R. Meyer *JCAP* **02** (2023) 056, [[arXiv:2209.13277](#)].
- [137] L. J. Hall, K. Jedamzik, J. March-Russell, and S. M. West *JHEP* **03** (2010) 080, [[arXiv:0911.1120](#)].